

**Real-time Method for Making Engine Exhaust Ash Measurements**

A THESIS

SUBMITTED TO THE FACULTY OF THE GRADUATE SCHOOL

OF THE UNIVERSITY OF MINNESOTA

BY

UDAYAN PATWARDHAN

IN PARTIAL FULFILLMENT OF THE REQUIREMENTS

FOR THE DEGREE OF

MASTER OF SCIENCE

DAVID. B. KITTELSON

August 2013



## **Acknowledgements**

This project was made possible through gifts by BP and Benjamin Liu. I would like to express my sincere gratitude to my advisor Prof. David Kittelson, who has provided continued support and encouragement through this project. His wealth of knowledge and passion for the subject infused a strong sense of curiosity in me, for which I am grateful. I would also like to thank Dr. Win Watts for his constructive feedback with my writings and help throughout the project. I am also grateful to Darrick Zarling for his help with the experiments.

Parts of this work were carried out in the Characterization Facility, University of Minnesota, which receives partial support from NSF through the MRSEC program.

## Abstract

Diesel particulate filters (DPF) are used to remove particulate matter (PM) from diesel engine exhaust. DPFs are regenerated periodically to oxidize the soot, leaving behind ash, which is the non-combustible portion of the PM. Ash build up in the DPF causes an increase in back pressure. This in turn, decreases fuel economy, increases cleaning frequency and contributes to degradation of DPF performance. Primary sources of diesel ash emissions are metallic additives present in the lube oil, fuel borne additives and engine wear metals.

The high temperature oxidation method (HTOM) was developed at the University of Minnesota to measure ash emissions in real time. HTOM utilizes a tube oven that combusts the PM present in the exhaust leaving behind the non-combustible portion, which is measured in real time with instruments such as the engine exhaust particle sizer (EEPS).

A series of experiments were performed to examine survival of ash components passing through the oven and the morphology of the particles leaving the oven. Morphology and limited composition information were obtained by collecting samples for Transmission Electron Microscopy (TEM) and Energy Dispersive Spectroscopy (EDS) analysis. The aerosol sources used for these experiments were sprays of lubricating oils with specially formulated additive packages and aqueous sprays of likely ash constituents. Atomized lube oils were only used for qualitative experiments because it was difficult to determine the loss of volatiles and thus the concentration additives upstream of the oven. TEM images of the samples indicated that calcium additized oils, containing 3700-3900 ppm Ca, produced particles in the size range of 5-50 nm; while a magnesium additized oil containing 500 ppm Mg, displayed a size range of 5-30 nm. Zinc additized oil, containing 1000 ppm Zn produced the lowest concentrations downstream of the oven and the smallest particles, in the size range of 5-20 nm.

The aqueous salt spray experiments were conducted to determine the survival of likely ash constituents in the HTOM. Salts of calcium, magnesium and zinc were atomized in water solutions and particle concentrations measured upstream and downstream of the oven. Survival fraction for the salts were found to be 54.7% for  $\text{CaSO}_4$ , 34.6% for  $\text{MgSO}_4$ , 26% for  $\text{Zn}_3(\text{PO}_4)_2$  and 7% for  $\text{ZnSO}_4$ .

Experiments were then conducted using actual diesel engine exhaust particles as an aerosol source. The objectives of these experiments were to determine the morphology and composition of the particles leaving the oven and estimate the engine ash emissions. Engine ash samples were collected at 250 N-m torque load and 1400 RPM. Total particle concentrations were measured with an SMPS. The TEM samples showed particles in the size range 5-100 nm and EDS analysis indicated that they consisted of mainly calcium and oxygen. The SMPS measurements were corrected for losses assuming CaO was the main ash constituent and indicated an exhaust ash content of  $44.3\mu\text{g}/\text{m}^3$  which corresponds to about 0.3 % of the exhaust PM.

## Table of Contents

List of Figures .....	vi
List of Tables .....	viii
List of Abbreviations .....	ix
Chapter 1: Introduction.....	<b>1</b>
1.1 Importance of ash emissions .....	1
1.2 Sources of ash emissions in diesel engines.....	2
1.3 Lube oil consumption & ash production .....	3
1.4 Objectives .....	11
1.5 Approach .....	11
Chapter 2: Apparatus .....	<b>13</b>
2.1 Atomizer .....	14
2.2 Catalytic stripper.....	15
2.3 Oven .....	15
2.4 Thermal precipitator.....	15
2.5 Scanning mobility particle sizer .....	18
2.6 Engine .....	19
2.7 Transmission electron microscope - Tecnai T-12.....	19
Chapter 3: Setup and procedure.....	<b>20</b>
3.1 Calibration experiments .....	20
3.1.1 Lube oil spray experiment.....	20
3.1.2 Aqueous salt spray experiment .....	22
3.2 Engine Ash experiment .....	24
3.3 TEM analysis - Statistical Sampling Procedure .....	25
Chapter 4: Results and Discussion.....	<b>26</b>
4.1 Atomized lube oil spray experiment results and discussion .....	26
4.2: Calibration experiment with aqueous salt sprays.....	38
4.2.1 Zinc sulfate penetration results .....	40
4.2.2 Zinc phosphate penetration results .....	42
4.2.3 Magnesium sulfate penetration results .....	44
4.2.4 Calcium sulfate penetration results.....	46
4.3 Engine ash experiment .....	49

Chapter 5: Conclusions and suggestions for future work -----	<b>56</b>
5.1 Conclusions -----	<b>56</b>
5.2 Suggestions for future work -----	<b>58</b>
Bibliography: -----	<b>59</b>
Appendix I -----	<b>64</b>
Appendix III -----	<b>67</b>
Appendix IV -----	<b>68</b>

## List of Figures

Figure 1: Flow through a DPF (Courtesy of Corning Inc.).....	1
Figure 2: Typical composition and structure of engine exhaust particles (Kittelson, 1998) .....	3
Figure 3: Typical composition and structure of engine exhaust particles (Whitby and Cantrell, 1976; Kittelson, 1998).....	4
Figure 4: A) Typical diesel soot agglomerate, B) Overlapping carbon structures.....	5
Figure 5: A) Schematic model of microstructure of the diesel soot particle (Ishigro et al., 1997). B) HRTEM image of diesel soot particle (Vanderwal et al., 2006).....	5
Figure 6: TEM images of cerium laden soot particles (Jung et al., 2005) .....	6
Figure 7: Change in metal concentration in sump oil over time (Givens et al., 2005) .....	7
Figure 8: Elemental distribution of Ca, Mg, Fe, P, Zn and O on ash particle.....	8
Figure 9: Ash samples at various stages of heating from 25 <sup>0</sup> C to 1150 <sup>0</sup> C (Sappok et al., 2009) ....	9
Figure 10: Overview of HTOM .....	13
Figure 11: Schematic of the atomizer (Gladis, 2010) .....	14
Figure 12: Schematic of the thermal precipitator initially used.....	16
Figure 13: Schematic of the thermal precipitator used for this study .....	17
Figure 14: Oil spray experiment setup.....	20
Figure 15: Schematic diagram of the calibration test setup for aqueous sprays .....	22
Figure 16: Engine ash experiment setup.....	25
Figure 17: Schematic of a TEM grid. A 6x6 square area at the center was chosen for sampling..	25
Figure 18: Upstream and downstream number concentration for different blends of lube oil (Upstream concentrations are measured after the CS).....	28
Figure 19: Volume weighted size distributions for different blends of lube oil .....	29
Figure 20: Number weighted size distribution for different blends of lube oil.....	31
Figure 21: TEM images of sample 100A (Ca/P/S) downstream of the oven.....	32
Figure 22: Number weighted size distribution for sample 100A (Ca/P/S) .....	32
Figure 23: TEM images of sample 101A (Zn/S/P).....	33
Figure 24: Number weighted size distribution for sample 101A (Zn/S/P) .....	33
Figure 25: TEM images of sample 102A (Ca/S) .....	34
Figure 26: Number weighted size distribution for 102A (Ca/S).....	34
Figure 27: TEM images of sample 103A (Mg/B).....	35
Figure 28: Number weighted size distribution for sample 103A (Mg/B).....	36
Figure 29: TEM images of John Deere lube oil.....	36
Figure 30: EDS analysis of the particle (on the right) showed the presence of Ca and Mg .....	36
Figure 31: Comparison of TEM images between different lube oils.....	37
Figure 32: Volume concentration of ZnSO <sub>4</sub> as a function of temperature.....	39
Figure 33: Volume weighted size distribution for zinc sulfate at 25 <sup>0</sup> C, 800 <sup>0</sup> C and 1150 <sup>0</sup> C (Upstream concentration is measured after the CS).....	41
Figure 34: Volume fraction vs temperature for zinc sulfate .....	41



Figure 35: Volume weighted size distributions for zinc phosphate(Upstream concentration is measured after the CS).....	42
Figure 36: Volume fraction vs temperature of zinc phosphate.....	43
Figure 37: Volume weighted size distributions for magnesium sulfate (Upstream concentration is measured after the CS).....	44
Figure 38: Volume fraction vs temperature for magnesium sulfate .....	45
Figure 39: Volume weighted size distributions for calcium sulfate (Upstream concentration is measured after the CS).....	46
Figure 40: Volume fraction vs Temperature for Calcium Sulfate .....	47
Figure 41: Number weighted size distribution at 250 N-m and 1400 RPM .....	50
Figure 42: Volume weighted size distribution at 250 N-m at 1400 RPM .....	51
Figure 43: TEM Images of ash particles at 250 N-m, 1400 RPM .....	53
Figure 44: Number, volume and mass weighted size distributions for engine exhaust at 250 N-m and 1400 RPM .....	55
Figure 45: Top part of the thermal sampler .....	64
Figure 46: Brass plate used between the two blocks .....	64
Figure 47: Bottom part of the thermal sampler.....	65
Figure 48: TEM images of zinc phosphate spray .....	68

## List of Tables

Table 1: Engine Specifications .....	19
Table 2: Different blends of lube oil provided by British Petroleum (Units are in ppm) .....	21
Table 3: Salts used for the calibration experiments .....	23
Table 4: Lube oil concentrations in PPM for different blends of lube oil .....	27
Table 5: Volume fraction for different blends of lube oil.....	30
Table 6: Summary of volumetric fraction survival at different temperatures.....	48
Table 7: Summary for mass and volume concentrations .....	52
Table 8: EDS analysis - element weight percentage (Average of 30 samples).....	53
Table 9: Typical lube oil composition in PPM .....	54
Table 10: Test matrix .....	66
Table 11: Results of EDS analysis for zinc phosphate sprays .....	68

## List of Abbreviations

BP	British Petroleum
CPC	Condensation particle counter
CS	Catalytic stripper
DPF	Diesel particulate filter
DMA	Differential mobility analyzer
EDS	Energy dispersive spectroscopy
EPA	Environmental Protection Agency
FTIR	Fourier transform infrared spectroscopy
GPF	Gasoline particulate filter
HRTEM	High resolution transmission electron microscope
HTOM	High temperature oxidation method
PM	Particulate matter
PPM	Parts per million
SEM	Scanning electron microscope
SMPS	Scanning mobility particle sizer
SI	Spark Ignition
TEM	Transmission electron microscope
TGA	Thermogravimetric analysis
TP	Thermal precipitator
ZDDP	Zinc dialkyldithiophosphate

## Chapter 1: Introduction

### 1.1 Importance of ash emissions

The United States Environmental Protection Agency (EPA) mandated that heavy-duty diesel trucks must meet stringent emissions standards for particulate matter (PM) and other pollutants (<http://www.epa.gov/otaq/standards/heavy-duty/hdci-exhaust.htm>). To meet the emission standards set by the EPA, it became necessary for the engine manufacturers to use after-treatment devices such as a diesel particulate filter (DPF) alone or in combination with other devices. A DPF cleans the exhaust of PM by using filters made of cordierite or other materials such as silicon carbide. It is used in-line with the exhaust on diesel engines. As seen in Figure 1, the DPF contains inlets that are plugged at the ends in an alternate fashion, forcing the exhaust to pass through the filter wall causing the PM to be deposited on the walls. The collected PM consists primarily of soot and ash.

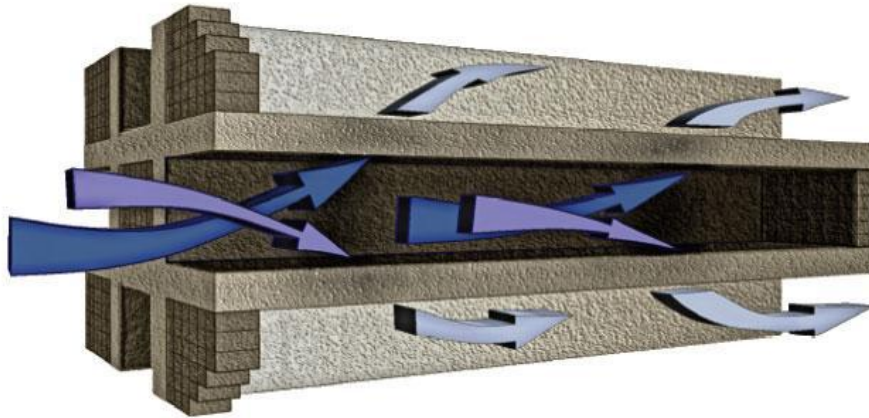


Figure 1: Flow through a DPF (Courtesy of Corning Inc.)

DPF's are periodically regenerated to oxidize the soot, thus reducing the backpressure, but ash tends to accumulate in the filters, as it is the non-combustible portions of the PM. Ash build up causes an increase in the back pressure causing a reduction in fuel economy and degradation in the performance of the DPF. Ash emissions also affect spark ignition (SI) engines by poisoning the 3-way catalyst loading gasoline particulate filters (GPF).

Hence, it is important to understand the physical and chemical composition of ash and the factors that influence ash emissions including: engine design and operating conditions, lubricating oil composition, fuel composition, and engine wear.

## **1.2 Sources of ash emissions in diesel engines**

In 2007, a total of 37.2 billion kg of lubricating oil was consumed worldwide. Fifty six percent of this was used for automotive applications (Mang et al., 2010). Lubricating oil contains metallic additives which enhance the properties of the oil. Some of the commonly used metallic additives are calcium and magnesium detergents and zinc dialkyldithiophosphate (ZDDP). Calcium detergents are added to the oil for piston deposit and corrosion control (Gardiner & Denison, 1940). ZDDP is used to protect oil from oxidation and reduces friction and wear (Asseff, 1941). These fundamental additives in combination with other additives extend reliability and durability of diesel engines (McGeehan et al., 2012). These additives are primarily responsible for the presence of ash in the engine exhaust (Bardasz et al., 2005). Analysis done on ash collected in a DPF has shown that ash is primarily composed of metallic compounds including sulfates, phosphates and oxides (Takeuchi et al., 2003, Young et al., 2004). Additional sources of ash present in the diesel engine exhaust besides lubricating oil additives are as follows (Sappok & Wong, 2007).

- Fuel-borne catalysts like cerium used to promote DPF regeneration.
- Metals from engine and exhaust system corrosion.
- Trace metals in conventional diesel fuel (Konstandopoulos et al., 2006; MECA, 2005).
- Engine-wear metals (Mayer et al., 2010).

The ash fraction for a conventional diesel engine ranges from 0.5% - 1.5% of diesel particulate matter (Sappok & Wong, 2007).

### 1.3 Lube oil consumption & ash production

Diesel exhaust particles consist mainly of highly agglomerated solid carbonaceous material, ash, volatile organic and sulfur compound as shown in Figure 2 (Kittelson, 1998). The solid particles consist of carbon and lube oil metal additives whereas the volatile portion of the PM is derived from un-burnt hydrocarbons originating from fuel and lube oil (Andrews et al., 1998).

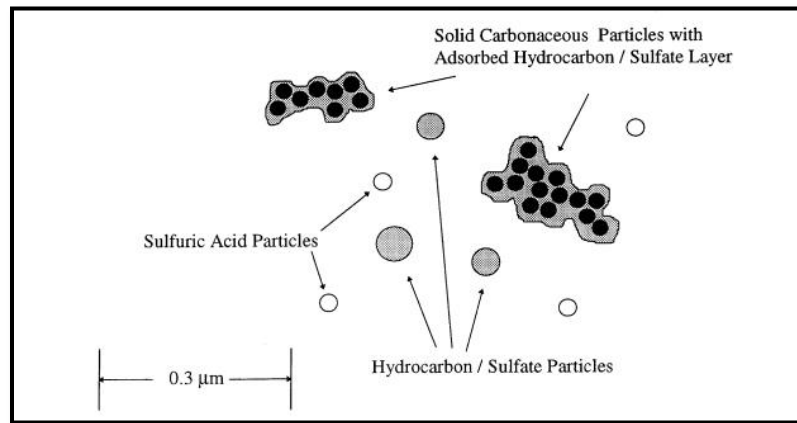


Figure 2: Typical composition and structure of engine exhaust particles (Kittelson, 1998)

Idealized diesel exhaust particle number and mass size distributions are shown in Figure 3 (Whitby and Cantrell, 1976; Adapted by Kittelson, 1998). The trimodal distribution consists of the nucleation, accumulation and a coarse modes. Most of the particle mass exists in the accumulation mode which is typically in the range of 0.05-0.5 μm whereas the nucleation mode contains most of the of particle numbers in the size range of 0.005-0.05 μm. The size range of these modes and boundaries between them shifts depending on the engine, fuel, and operating conditions.

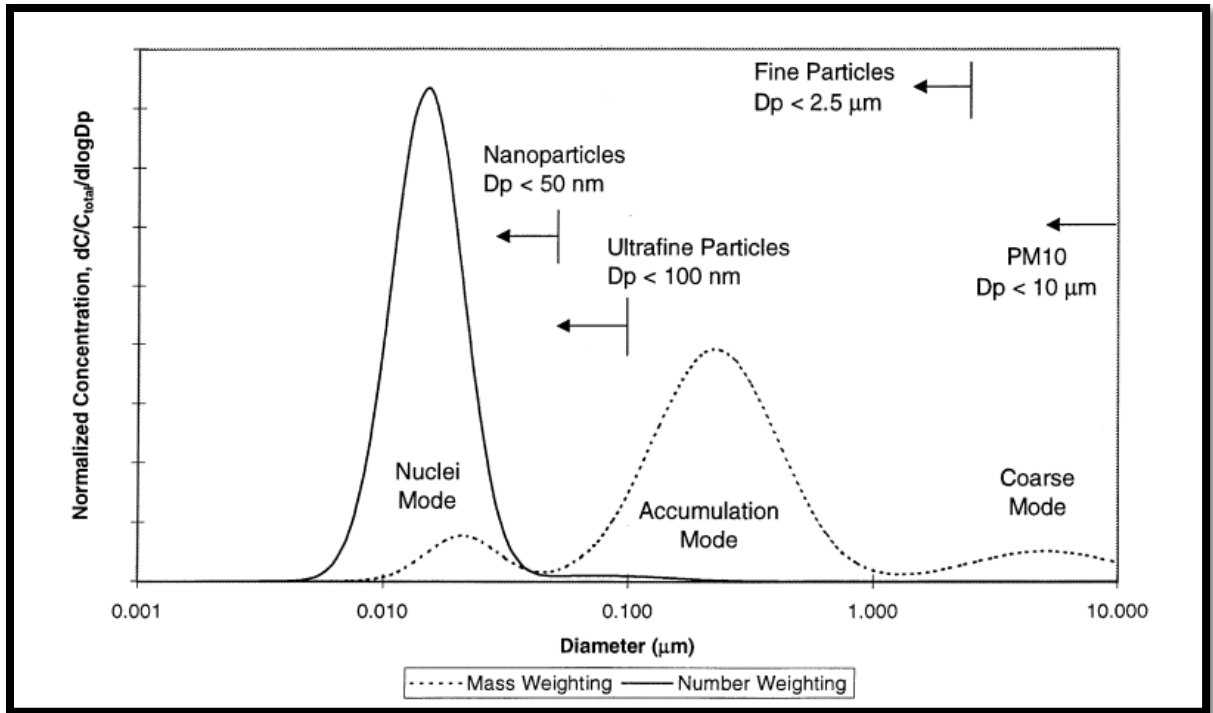


Figure 3: Typical composition and structure of engine exhaust particles (Whitby and Cantrell, 1976; Kittelson, 1998)

The accumulation mode contains carbonaceous agglomerates and associated adsorbed materials (Kittelson, 1998). A transmission electron microscope (TEM) image of a soot sample collected in the lab from the exhaust of a medium duty engine operating at intermediate speed and load is shown in Figure 4. Figure 4A depicts a typical diesel soot agglomerate, a long chain of carbonaceous material with adsorbed material 50-250 nm long. Figure 4B represents a magnified image of a soot particle, which shows the overlapping carbon structures. As described by Kittelson (1998), the nucleation mode mostly consists of volatile hydrocarbons along with solid carbon and metallic compounds derived from lubricating oil.

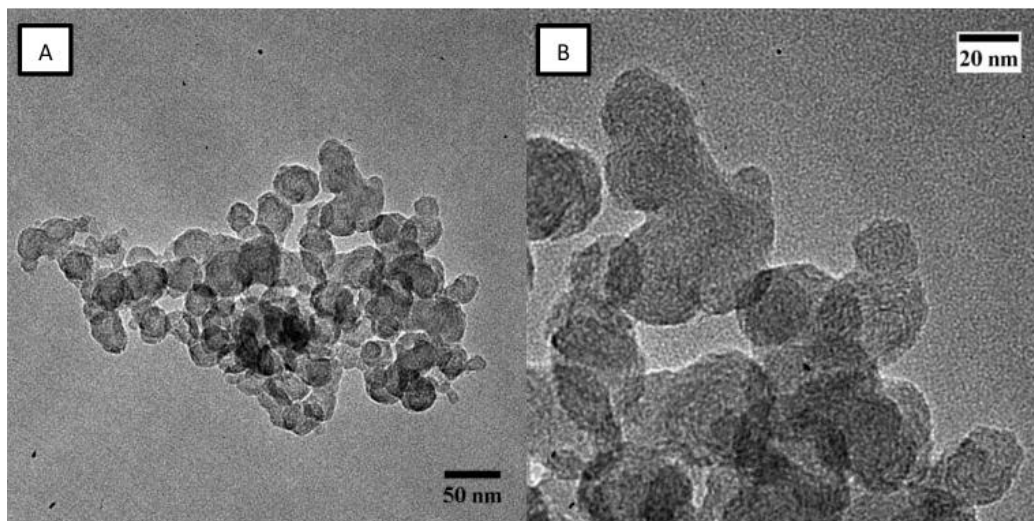


Figure 4: A) Typical diesel soot agglomerate, B) Overlapping carbon structures

Ishiguro et al. (1997) evaluated the microstructure of diesel soot particles and found that they contained a closed shell nucleus, which is at the center region of the fine particles as shown in Figure 5A. The nucleus is surrounded by multiple layers of networked carbon atoms. The high resolution transmission electron microscope (HRTEM) image of a soot particle can be seen in Figure 5B (Vanderwal et al., 2006) where multilayered carbon network is present.

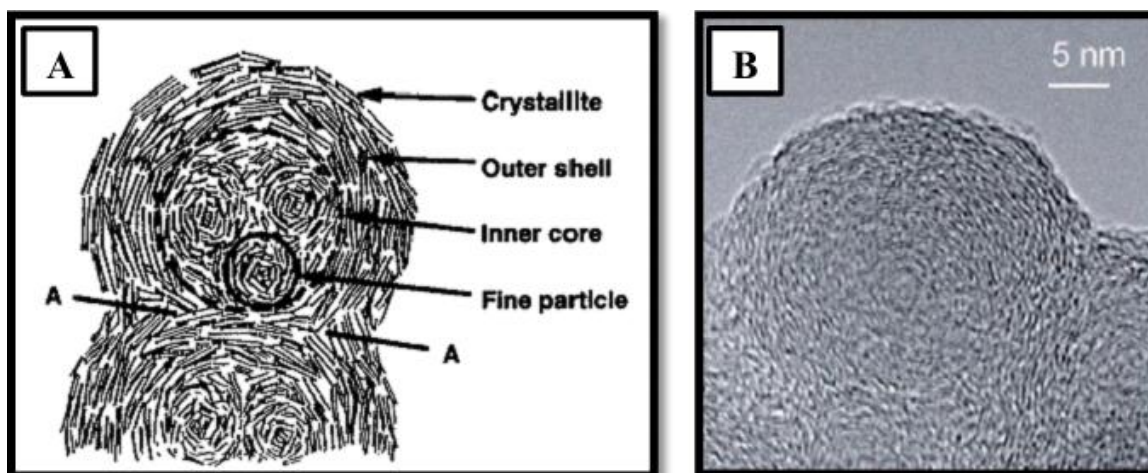


Figure 5: A) Schematic model of microstructure of the diesel soot particle (Ishiguro et al., 1997). B) HRTEM image of diesel soot particle (Vanderwal et al., 2006)



Jung et al. (2005) did a study on the influence of a cerium additive on diesel particulate matter emissions. For the study, the fuel was doped with cerium additive at dosing level of 25 ppm and 100 ppm. TEM images of soot samples showed cerium additive decorating the soot particle as shown in Figure 6.

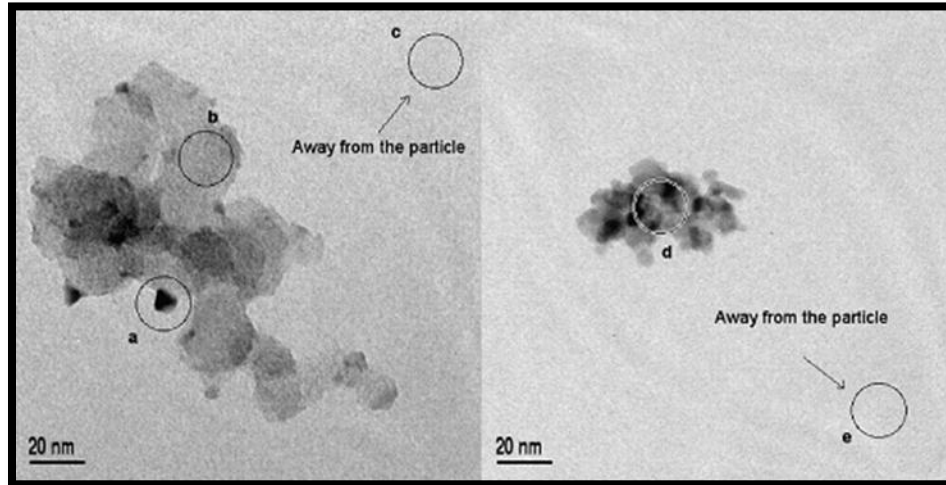


Figure 6: TEM images of cerium laden soot particles (Jung et al., 2005)

In Figure 6, the dark spots inside circles a and d indicate the presence of cerium on the soot particles. This suggests that metal additives found in lubricating oil tend to decorate soot particles (Jung et al., 2005).

Multiple studies have been conducted to find a relationship between lube oil consumption and ash production. The study performed by Bardasz et al. (2005) found that the ash found in the filter was less than expected based on the oil consumption rate. The amount of ash accumulated in the DPF as a percentage of the expected amount ranged from 35% (Bardasz et al., 2005) -70% (Givens et al.,2003). This result clearly suggests that a fraction of the ash deposits in the engine system. The reason for the difference in the actual ash and expected ash deposition on the DPF are attributed to the factors discussed below.

A) Ash forming additives do not volatilize at the same rate as the lighter base oil containing hydrocarbons (Chamberlin & Zalar, 1984).

This hypothesis is supported by the work conducted by Givens et al. (2003) who showed the change in concentration of different metals over time in Figure 7.

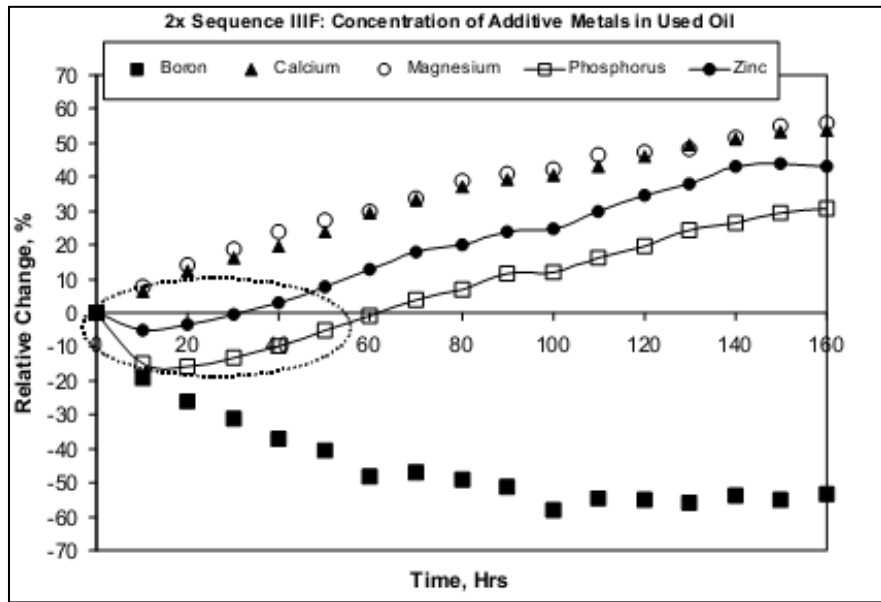


Figure 7: Change in metal concentration in sump oil over time (Givens et al., 2005)

In Figure 7, all metals except boron displayed an increase in concentration over time suggesting the evaporation of volatile component of the lubricating oil present in the sump. Givens et al. (2005) attributed the initial drop in concentrations of phosphorus and zinc to formation of surface film with the engine and then reaching an equilibrium with the base oil.

B) A part of the metal from the lubricating oil could deposit on the surface of the engine and the after-treatment systems. They could also react with the surfaces to form anti-wear films.

Some constituents of ZDDP present in the lubricating oil have high volatility (Fritzsche & Gerve, 1980). This causes ZDDP to decompose early in the oil's life and leads to reaction with surfaces of the engine to form a layer of phosphorus containing material creating a volatile zinc-containing by-product Givens et al. (2003). Hence, this leads to lower than expected zinc compounds to be present in the DPF sample.

Studies done on chemical composition of ash found in the DPF showed that calcium and phosphorus were the key elements present in the DPF (Takeuchi et al., 2003). They also found no boron in the DPF sample concluding that boron doesn't affect the performance of the DPF. Liati et al. (2011) performed a transmission electron microscope (TEM) and scanning electron microscope (SEM) analysis of diesel ash particulate matter deposited in the DPF. The ash agglomerates were mostly round and consisted of additive metals in the form of sulfates, phosphates and oxides. Sappok and Wong (2007) conducted TEM analysis on ash samples collected on 47 mm glass fibers filters and found the presence of lubricating derived elements like Ca, Mg, Zn and P as shown in Figure 8.

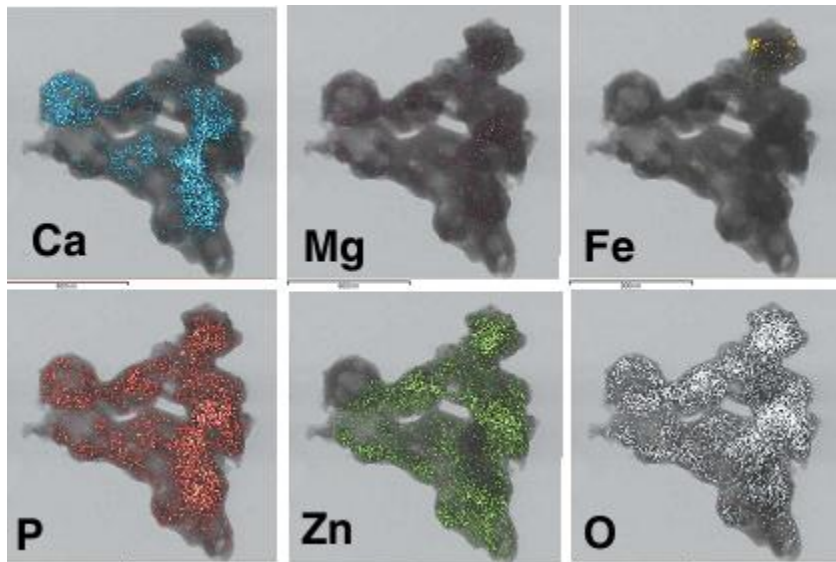


Figure 8: Elemental distribution of Ca, Mg, Fe, P, Zn and O on ash particle

Lubricating oil manufacturers are facing the challenge of producing an ash-less oil to reduce ash emissions and extend DPF life. McGeehan et al. (2012) tried to develop ash-less oil but found that the oil could not meet valve-train requirements of the API CJ-4 SN/ACEA E9 oil categories, however oil containing 0.3-0.4% sulfated ash was able to meet critical diesel and gasoline tests. Conventional CJ-4 oil contains 1.4% ash and 0.14% phosphorus.

Sappok et al. (2009) conducted experiments to study the effect of ash accumulation in DPFs. They heated ash collected in the DPF and saw that temperatures in excess of 900°C caused the morphology to change rapidly as the particles to sintered and fused together. Figure 9 shows ash samples after exposure to elevated temperatures (Sappok et al., 2009)



Figure 9: Ash samples at various stages of heating from 25<sup>0</sup>C to 1150<sup>0</sup>C (Sappok et al., 2009)

For temperatures above 1000°C, Sappok et al. (2009) found that Ca, Mg, S and P compounds go through phase changes, “whereas the level zinc oxide related phases increase significantly”. At temperature of 1150°C they found that calcium sulfate and magnesium zinc phosphate were the most abundant ash compounds remaining in the sample (Sappok et al., 2009).

A high temperature oxidation method (HTOM) was developed at University of Minnesota (Kim, 2005; Filice et al., 2007; Apple et al., 2009; Gladis, 2010). It is intended to measure ash emissions and approximate lube oil consumption in real time over transient engine conditions. Kim (2005) performed experiments to test the feasibility of measuring ash content of engine exhaust using HTOM. Kim (2005) dosed the fuel with 1% lubricating oil of a known metal content and found the survival of metallic ash components to be 47%. He suggested ash deposition on the internal surfaces of the engine and particle evaporation in the tube furnace to be the reason behind low ash recovery.

To calibrate the HTOM, Filice et al. (2007) conducted experiments with  $\text{MgCl}_2$  and  $\text{MgSO}_4$  particles for tube oven temperatures ranging from 25°C to 1100°C. Particle volume concentrations surviving the oven were found to be 94% for  $\text{MgCl}_2$  and 89% for  $\text{MgSO}_4$ . Gladis (2010) measured the survival of different blends of oil through the oven and over-predicted the volume fraction of calcium and magnesium. The measured to expected volume fraction, was reported to 2.51 and 1.48 for calcium and magnesium, respectively. The reason attributed to over prediction for calcium and magnesium was that activated carbon was removing a portion of the volatile fraction of lube oil in addition to butanol vapors causing an increase in metallic ash concentrations. Another possible reason pointed out by Gladis (2010) was that particles larger than the upper sizing limit of scanning mobility particle sizer (SMPS) were not counted causing the volume concentration of the oil sprays upstream of the oven to be underestimated. Downstream of the oven the particles were much smaller so that most of the volume was counted. This led to an overestimation of the ash fraction.

## **1.4 Objectives**

This thesis continues development of the HTOM by focusing on the fate of ash metals as they pass through the oven. The survival rate of metals has been examined using oil and aqueous sprays with an improved setup. A thermal precipitator (TP) was designed, built, and used to collect a relatively unbiased samples of the particles present upstream and downstream of the oven for TEM analysis.

The objectives of this thesis are:

1. Develop a sampling system to collect unbiased particle samples for TEM analysis.
2. Perform calibration experiments to measure the survival of different ash constituents.
3. Understand the morphology of ash produced from the oil spray experiments.
4. Collect samples of engine exhaust particles upstream and downstream of the HTM oven and determine the morphology of the ash and its chemical composition.

## **1.5 Approach**

Engine exhaust contains non-combustible particulate matter, which is derived from lube oil additives, engine wear metals and fuel borne additives (Sappok and Wong, 2007). To measure ash emissions, long run times are needed to collect measurable ash for analysis. To reduce the long sample time, the HTOM was developed to measure ash emissions in real time. The aim of the work described here is to improve our understanding of the HTOM.

The approach taken is described below.

Calibration experiments were performed to obtain quantitative estimates of the survival fractions of different lube oil additives. The results from the calibration experiments can be used to back-track the metallic additives present upstream of the oven, thus aiding in predicting metallic ash emissions in real time.

Lubricating oil experiments performed with specially blended oils were originally intended to calibrate the HTOM. The lube oils used for calibration contain known concentrations of metals like calcium, magnesium and zinc. The concentration of the atomized lube oil can be measured upstream and downstream of the oven with the help of the SMPS. However, it was difficult to determine the concentration of metals upstream of the oven because of losses of volatile material from the lube oil sprays. Consequently the lube oil spray experiments have only been used for qualitative analysis. Instead, aqueous salts sprays were used for calibration experiments.

For aqueous salt spray experiments, atomized aqueous solutions of metallic salts found in ash were used as an aerosol source. Particle concentrations upstream and downstream of the oven were measured using the SMPS. This allowed survival fractions of different metal salts to be determined. These survival fractions can be used estimate upstream concentrations of ash in actual engine experiments.

Engine ash experiments used actual engine exhaust as an aerosol source. Measurements made downstream of the oven were corrected for losses using the results obtained from aqueous spray experiments to estimate the upstream concentration of ash.

## Chapter 2: Apparatus

The overview of the system used for the HTOM experiments is shown in Figure 10. It consists of a catalytic stripper (CS), followed by a quartz tube that passes through a high temperature oven. Downstream of the oven the flow passes through a length of tubing to cool it to ambient temperature before entering the sampling or measurement system. The CS is only used when it is necessary to remove combustible materials (typically butanol vapor) from the flow before entering the oven. The flow through the oven is controlled by downstream instruments and appropriate bypass flows to a nominal value of 1.0 L/min. The particles present downstream of the oven were sampled on TEM grids using a thermal precipitator and the concentration of the particles was measured using an SMPS. The key apparatus used for HTOM are explained in detail below.



Figure 10: Overview of HTOM



## 2.1 Atomizer

An atomizer was used to produce aerosols for the calibration experiments. The atomizer used for this study is a type of pneumatic atomizer which uses the energy from the compressed air to break up a liquid stream. The schematic of the atomizer used is shown in Figure 11.

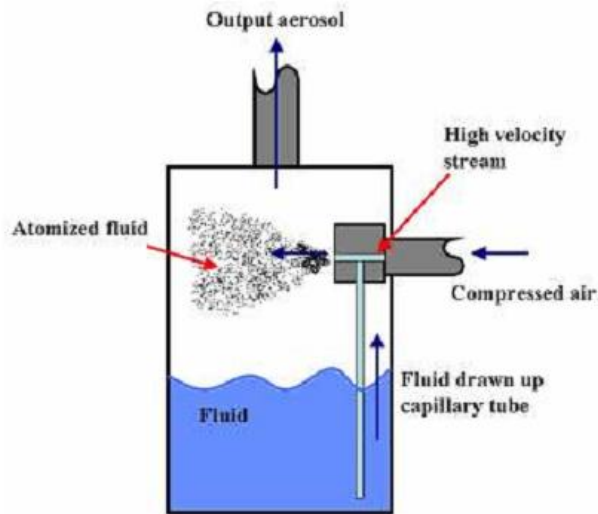


Figure 11: Schematic of the atomizer (Gladis, 2010)

Compressed air entering the atomizer is forced through a short nozzle. This creates a vacuum which causes the liquid to be sucked upwards. The shearing action of the compressed air causes the liquid to break into small droplets. The largest particles either settle out or are lost by collision with the opposite wall. The droplets have a mass mean diameter of 2.1-3  $\mu\text{m}$  (Hinds, 1999) when operated at a pressure of 140 kPa (20 psig). The atomizer for this study was run at a pressure of 275 kPa (40 psig). The droplet size used in the calculations was assumed to be 2.5  $\mu\text{m}$ .

The correlation of the particle size to the droplet size as given in Hinds is,

$$d_p = d_d (F_v)^{1/3}$$

Equation 1: Correlation of particle size and droplet size

where,  $d_p$  is the particle diameter,  $d_d$  is the droplet diameter and  $F_v$  is the volume fraction of the nonvolatile solute.

## **2.2 Catalytic stripper**

The catalytic stripper (CS) was invented at University of Minnesota by Khalek and Kittelson (1995). The primary purpose of the CS is to remove all the volatile components and moisture of the particles flowing through it. It consists of short section of oxidation catalyst like that used in exhaust after-treatment systems enclosed in a heated tube, followed by a copper cooling coil to reduce the temperature to ambient. In the work done here the catalyst was heated to a temperature of 320°C. It is used as a precautionary measure to prevent ignition of solvents or other combustibles present in the aerosol before it enters the high temperature oven

## **2.3 Oven**

The oven used for the experiment is a Carbolite CTF 12-65-550 tube oven, which has a maximum temperature of 1200°C and has a heated length of 550 mm and a diameter of 65 mm. These features allow for a heated length residence time of 1.4 s for a flow rate of 1 L/min at a temperature of 1100°C. 1 L/min flow rate ensures that the flow inside the oven is laminar.

High temperature insulation is packed in the ends of the furnace between the work tube and the inner diameter of the tube oven (Gladis, 2010).

## **2.4 Thermal precipitator**

A thermal precipitator was designed to obtain a representative sample of the particles upstream or downstream of the oven. The thermal precipitator works on the principle of thermophoresis. Hinds (1999) describes thermophoresis as the “movement of particle in the direction of decreasing temperature.” A thermal force is caused due to greater transfer

of momentum from the molecules on the hot side relative to the cold side. The thermophoretic velocity is proportional to the temperature gradient and is given by equation 2 below:

$$V_{th} = \frac{-0.55\mu \nabla T}{\rho_g T_b}$$

Equation 2: Thermophoretic velocity

Where,  $\nabla T$  represents the temperature gradient,  $\rho_g$  represents the density of the aerosol and  $T_b$  represents the bulk mean temperature.

In a thermal precipitator a temperature gradient is applied to the sample and particles deposit on a cool surface. Initially, for this project, a precipitator was designed whose schematic is shown in Figure 12.

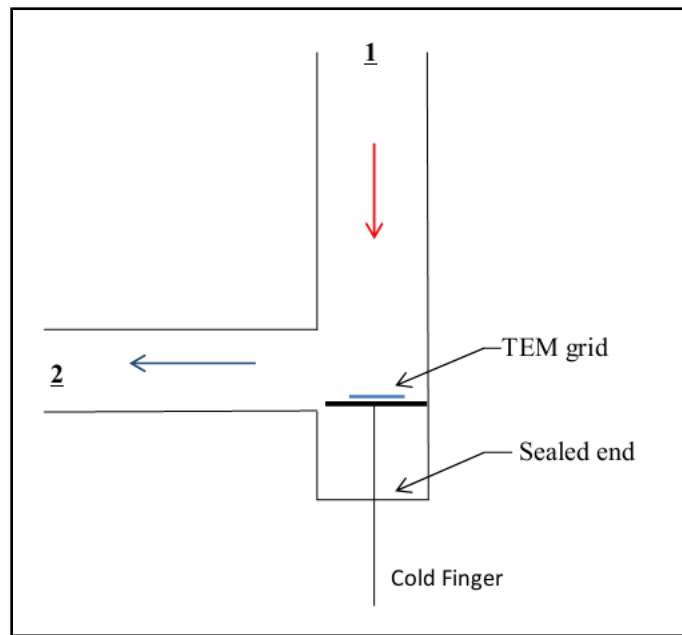


Figure 12: Schematic of the thermal precipitator initially used

The aerosol entered the “inverted L” section at 1 and exited at 2. The TEM grid was taped to a copper rod which was cooled using an ice bath. The temperature difference between the aerosol and the TEM grid caused the particles to deposit on the TEM grid. Due to a small temperature gradient, the precipitator had poor deposition efficiency.

To improve deposition efficiency, a new thermal precipitator was designed, based on the work of Lorenzo et al. (2007). It is shown in Figure 13 and detailed drawings are given in Appendix I.

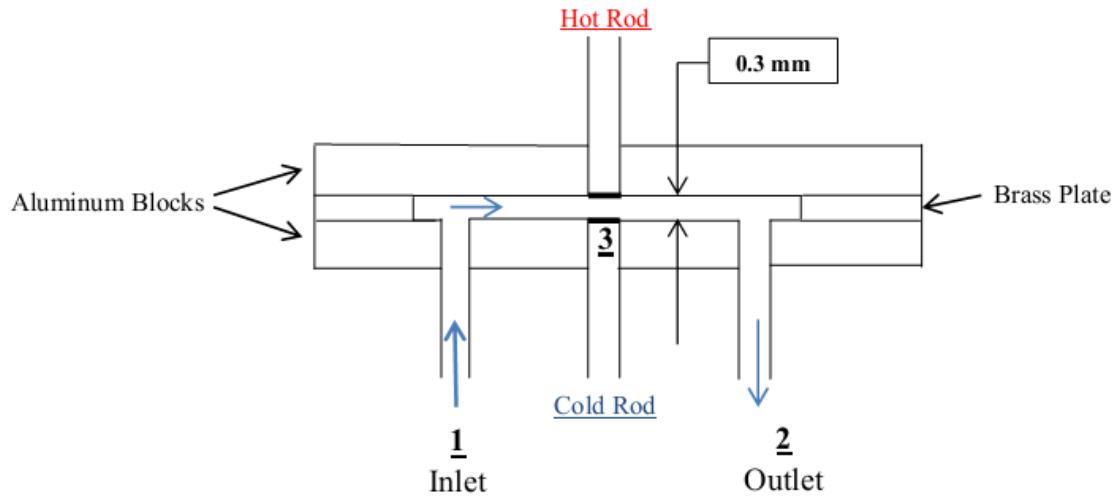


Figure 13: Schematic of the thermal precipitator used for this study

. The new design enhanced thermophoretic deposition due to an increased temperature gradient. It also helped in better handling of the TEM grids. This improved the overall specimen quality and ensured minimum contamination. All the forceps and grid boxes used during the sampling were stored in a clean and dry space.

As seen in Figure 13, the aerosol enters the precipitator vertically at 1 and then moves along the length of the block and exits at 2. Midway, a TEM grid placed at 3, on a copper rod cooled using an ice bath. Directly above is a hot copper rod maintained at 373 K. The two copper rods are flush with the aluminum blocks. The aluminum blocks are separated by a 0.3 mm thick brass plate which acts as a seal between the two blocks and the cutout provides space for the aerosol to flow.

The aluminum block has a threaded hole at the center to insert and remove the TEM grid on a copper rod. This arrangement ensures correct alignment of the surface with that of the block and allows easy removal and insertion of the TEM grid. The copper rod on

which the TEM grid placed has a circular notch 3.2 mm in diameter. The notch helps keep the TEM grid in place. The end of the copper rod is immersed in ice water for cooling. Another copper rod placed opposite to the TEM grid. It was heated to a temperature of 373 K using a heat tape. A temperature controller maintained temperature to  $\pm 1$ K. PTFE tubing thermally isolated the copper rods from the aluminum block. The distance between the copper rods could be adjusted. For this study, it was kept constant at 0.3 mm.

## **2.5 Scanning mobility particle sizer**

A scanning mobility particle sizer (SMPS) was used to measure the aerosol size distribution. It consists of a differential mobility analyzer (DMA) which segregates particles based on mobility diameter and a condensation particle counter (CPC) which measures the concentration of the particles. The TSI 3081 DMA and 3776 CPC were used for this study. The 3776 CPC is capable of measuring concentrations in the range of  $10$ - $10^7$  particles/cm<sup>3</sup>. The 3081 DMA can measure mobility diameter in the range of 0.0025-1  $\mu$ m. The range of the DMA is a function of the sheath flow rate and aerosol flow rate. For this study, the sheath flow rate was fixed at 10 L/min and the aerosol flow rate at 1.5 L/min allowing a sizing range of 7.23 nm - 294.3 nm.

## 2.6 Engine

The engine used in this study is a model year 2005 John Deere 4045H engine meeting EPA tier 2 off-highway emissions standards. It is a 4 cylinder, 4.5 L, turbocharged direct injection diesel engine rated at peak power of 129 kW (173 HP) at 2400 RPM and peak torque of 645 N-m at 1500 RPM. The engine was operated at steady speeds and

Table 1: Engine Specifications

### John Deere 4045H

Number of cylinders	4
Displacement, L (cu-in)	4.5 (275)
Bore and Stroke (mm)	106 x127
Compression ratio	17.0:1
Engine type	In line, 4 cycle
Aspiration	Turbocharged and air to air cooled

## 2.7 Transmission electron microscope - Tecnai T-12

The transmission electron microscope (TEM), Tecnai T-12, was used for analyzing specimens collected in this study. It has lanthanum hexaboride (LaB<sub>6</sub>) as the source and has accelerating voltage ranging from 20 to 120 kV. The Tecnai T-12 can provide magnifications up to 700,000x and has a point resolution of 0.34 nm and a line resolution of 0.2 nm. The TEM is also equipped with INCA energy dispersive spectrometer (EDS), which can be used to detect elements from beryllium to uranium.

### Chapter 3: Setup and procedure

The experimental setup and procedures discussed below are: calibration experiments using lube oil and aqueous sprays, engine ash experiments and TEM procedures. The test matrix is in Appendix II.

#### 3.1 Calibration experiments

The goal of calibration experiment is to estimate the survival fraction of metal additives surviving the oven. The following calibration experiments were performed.

##### 3.1.1 Lube oil spray experiment

The lube oil spray experiment consists of an atomizer to atomize a solution of oil in butanol. The concentration of oil in the butanol determines the size of the droplet of oil after butanol has evaporated. For the oil spray experiment, the concentration of oil was 1% by volume for all the blends of the oil in butanol. The setup for the experiment is shown below in

Figure 14.

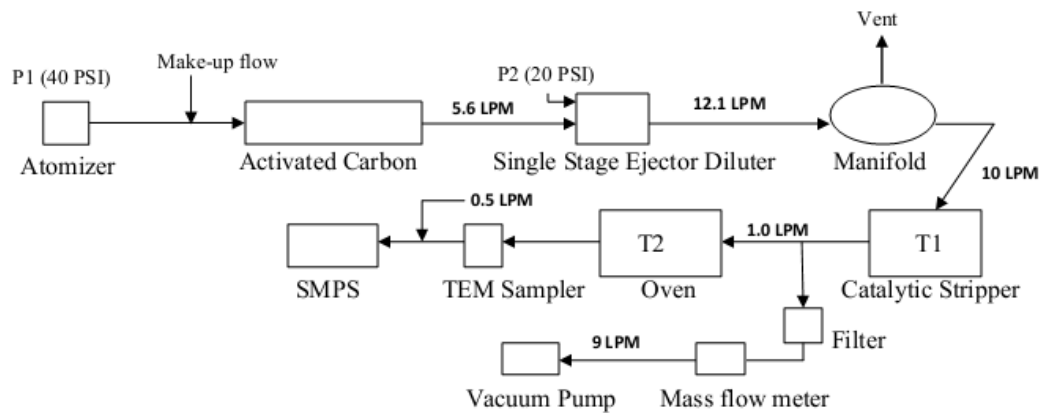


Figure 14: Oil spray experiment setup

Upon atomization, the aerosol passed through a column of activated charcoal which adsorbs butanol. The aerosol was then diluted by a factor of 2.7 in the an AirVac AVR062H. The AVR062H is a single stage vacuum pump which produces a maximum vacuum flow rate of 11.9 L/min and a maximum exhaust flow of 23.2 L/min. The exhaust of the ejector diluter was then fed to the manifold. From the manifold, a flowrate of 10 L/min was pulled in through the CS. The CS was used as a precautionary measure to prevent possible ignition of butanol vapors in the oven. 1 L/min of aerosol was pulled in through the oven which is maintained at 1150<sup>0</sup>C. High temperature causes the combustible components to burn, leaving only ash. The ash is sampled using a thermal precipitator (TP). The sampling time for ash was 25 min for each oil spray experiment. The atomizer pressure was set at 276 kPa (40 psi) and the pressure to the ejector-diluter was set at 138 kPa (20 psi). The blends of lube oil provided by BP have the following metals present as shown in Table 2.

Table 2: Different blends of lube oil provided by British Petroleum (Units are in ppm)

<b>Oil blend</b> <b>Element</b>	<b>104A</b> <b>(Base Oil)</b>	<b>100A</b>	<b>101A</b>	<b>102A</b>	<b>103A</b>
<b>B</b>	<5	<5	<5	<5	285
<b>Ca</b>	<2	3946	<2	3724	<2
<b>Mg</b>	<2	8	<2	<2	~500
<b>P</b>	2	1052	976	13	<10
<b>S</b>	55	802	1998	8804	57
<b>Zn</b>	<5	<5	1008	<5	<5



### 3.1.2 Aqueous salt spray experiment

A schematic overview of the calibration test setup is shown in Figure 15. Salt solutions were prepared according to recipes that would produce salt particles 50 nm in diameter (equation 1). Fifty nanometers was chosen as the particle diameter because it is in the same size range as typical engine exhaust aerosols. The atomizer was cleaned thoroughly each time the salt solution was changed using triple rinses of deionized distilled water and isopropyl alcohol. A zero check was performed before each experiment by replacing the atomizer with a HEPA filter. The SMPS was used to measure particles and scans were performed until three consecutive scans displayed zero particle count.

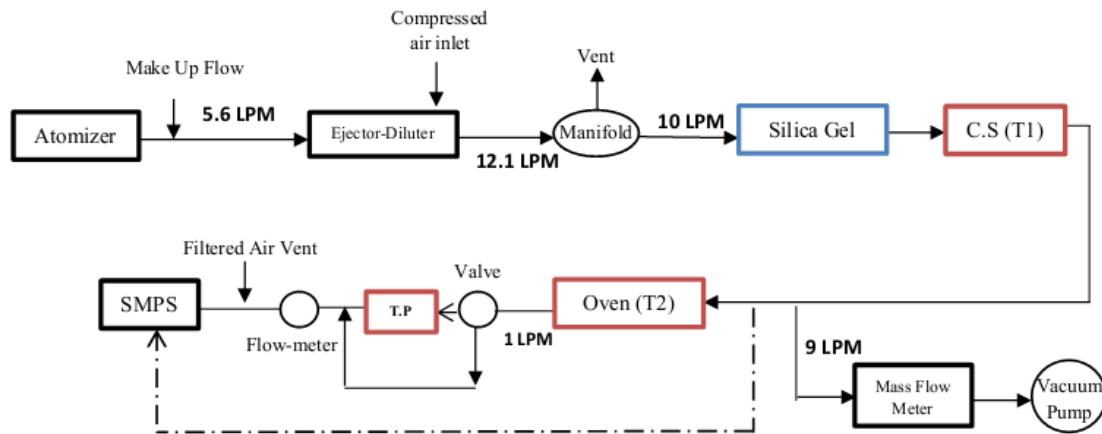


Figure 15: Schematic diagram of the calibration test setup for aqueous sprays

To get high concentrations of the aerosol, the operating pressure of the atomizer and the ejector diluter were selected such that the dilution of the aerosol was minimized. The atomizer was run at a pressure of 276 kPa (40 PSI) and the ejector diluter was operated at a pressure of 138 kPa (20 PSI). The exhaust of the ejector diluter consisting of the atomized sample diluted with filtered compressed air was the input to the vented manifold shown in Figure 15. Flows were adjusted by values as shown in Figure 15 with appropriate venting and make up flows as required. Flow through the catalytic stripper

(CS) was maintained at its design flow of 10 L/min and flow through the oven at 1 L/min. After leaving the distribution manifold the sample flow passed through a silica gel diffusion dryer to remove water and then through the CS for final drying. The CS was operated at a temperature of 320°C. The aerosol particle size distribution was measured upstream and downstream of the oven using an SMPS. Upstream and downstream measurements were not made simultaneously but were measured alternately because only one SMPS was available. The thermal precipitator (TP) was bypassed except when TEM samples were taken. The dotted line in Figure 15 shows the point where upstream particle number concentration was measured, which is after the CS. The salts used for the calibration experiments are as shown in Table 3. Each experiment was performed at least three times to evaluate for repeatability. The repeats were performed on three different days.

Table 3 summarizes the salts used for the experiment.

Table 3: Salts used for the calibration experiments

Salts	Solvent	Density of Salt (g/cc)	Density of Solvent (g/cc)	Salt needed to create 50 nm particles in 1 liter of solvent (mg)
ZnSO <sub>4</sub> (Hexahydrate)	Water	2.072	1	16.576
Zn <sub>3</sub> (PO <sub>4</sub> ) <sub>2</sub> (Hydrate)	Water	3.998	1	31.984
MgSO <sub>4</sub> (Anhydrous)	Water	2.66	1	21.28
CaSO <sub>4</sub> (Anhydrous)	Water	2.96	1	23.68

### 3.2 Engine Ash experiment

The setup for the engine ash experiment is shown in Figure 16. The John Deere 4045 T engine was run at a steady state operating point of 250 N-m at 1400 RPM. The exhaust from the engine was diluted using a single stage ejector diluter similar to the first stage of the dilution system described by Abdul-Khalek (1999). Filtered, dried compressed air was used to dilute the exhaust. The ejector diluter was operated at a pressure of 276 kPa (40 PSI) to give a dilution ratio of 4.3. The dilution ratio was measured using an AVL SESAM Fourier transform infrared spectroscopy (FTIR) gas analyzer. The ratio of NO concentration upstream to downstream of the ejector diluter determined the dilution ratio. The exhaust was then passed through an oven maintained at 1150°C at a flow rate of 1 L/min. A thermal precipitator was used to collect TEM samples downstream of the oven. Additional dilution occurs after the flow meter with a make-up flow of 0.5 L/min added to match the flow of the SMPS. The SMPS was used to measure the exhaust particle size distribution upstream and downstream of the oven.

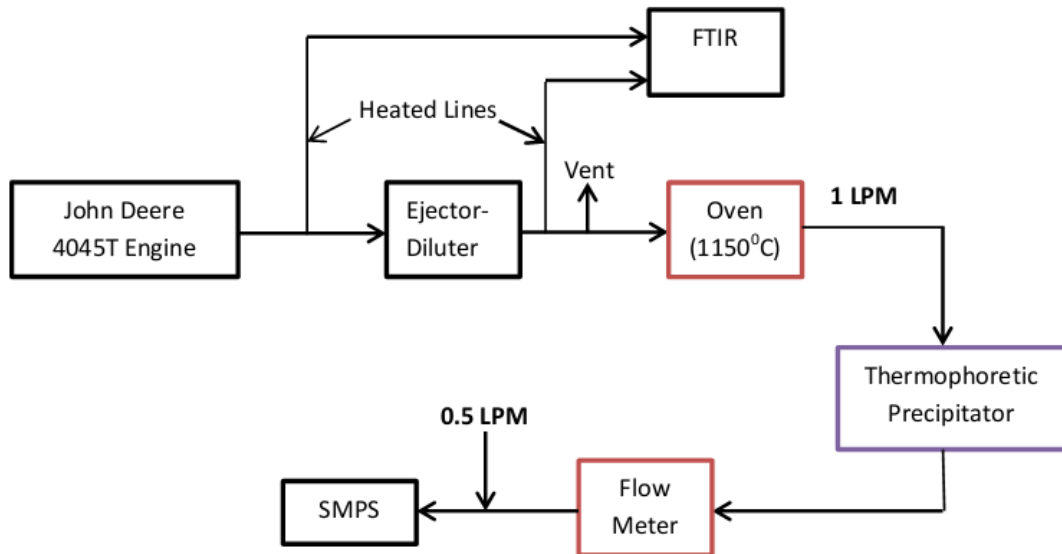


Figure 16: Engine ash experiment setup

### 3.3 TEM analysis - Statistical Sampling Procedure

The TEM grids were 300 mesh copper grids with a carbon film. The TEM grid and its meshes can be seen on a computer screen and points of interest can be marked. Out of the 300 meshes, 36 meshes square grid were created by marking a 6 x 6 square with numbers from 1-36 around the center of the TEM grid as shown in

Figure 17. Ten meshes were chosen at random from marked 36 meshes using a random number generator. EDS and TEM analysis were performed on each of the randomly chosen meshes. TEM imaging was performed at a magnification of 18500x.

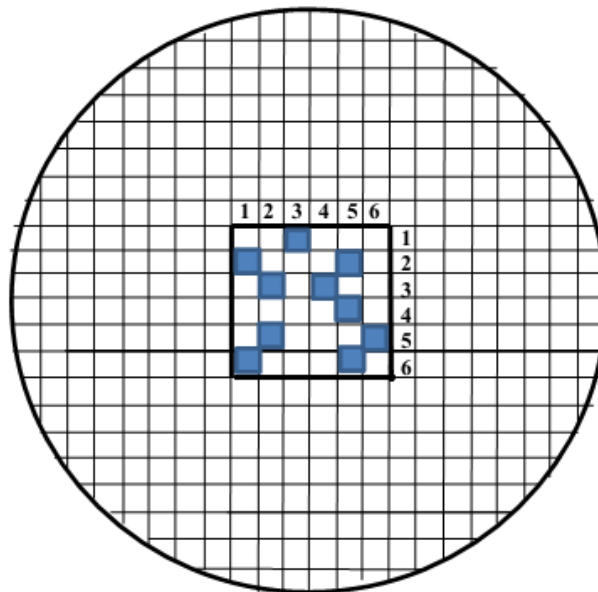


Figure 17: Schematic of a TEM grid. A 6x6 square area at the center was chosen for sampling

## **Chapter 4: Results and Discussion**

### **4.1 Atomized lube oil spray experiment results and discussion**

This section provides a qualitative understanding of the survival and the morphology for particles present in the specially blended lube oils. The setup and the procedure followed for the oil spray experiment is explained in detail in section 3.1.1. Initially, the objective of the lube oil spray experiment was to obtain a quantitative estimate on the survival of lube oil constituents as they pass through the oven maintained at 1150°C using an approach similar to that used by Gladis (2010). To determine a correct estimate of the survival fraction, it is essential to know the concentration of the metal additive upstream of the oven. Gladis (2010) assumed that lube oil solutions in butanol after drying in diffusion dryer consisted of pure lube oil with a known concentration of additive but he did not check the validity of this assumption. For the work described here, the lube oil spray experiments are not used to study the survival of the metallic additives but rather to study the composition and morphology of the particles present downstream of the oven. The lube oils used for these experiments were specially formulated blends provided by BP. The lube oil was mixed with butanol in a 1/100 ratio by volume. This ratio of lube oil to butanol would provide approximately 50 nm particles upon complete evaporation of butanol with no loss of volatile lube oil components (refer to equation 1). Under ideal conditions this would be the condition of the aerosols leaving the diffusion dryer but it is unlikely that this condition was actually achieved so this was merely taken as a convenient reference condition. No measurements were made at this condition and instead the only measurements made upstream of the oven were made at the exit of the CS. After being processed in the CS at 320°C only the least volatile components of the lube oil would be expected to remain. All data are corrected for thermophoretic losses by methods described in Appendix III.

Table 4 shows lube oil concentrations in PPM for different blends of lube oil used for the study. 100A and 102A are calcium base oil, 101A is zinc base oil and 103A is magnesium base oil.

Table 4: Lube oil concentrations in PPM for different blends of lube oil

<b>Oil blend</b> <b>Element</b>	<b>104A</b> <b>(Base Oil)</b>	<b>100A</b>	<b>101A</b>	<b>102A</b>	<b>103A</b>
<b>B</b>	<5	<5	<5	<5	285
<b>Ca</b>	<2	3946	<2	3724	<2
<b>Mg</b>	<2	8	<2	<2	~500
<b>P</b>	2	1052	976	13	<10
<b>S</b>	55	802	1998	8804	57
<b>Zn</b>	<5	<5	1008	<5	<5

Figure 18 shows a plot of total volume concentration of particles with time, upstream and downstream of the oven maintained at 1150°C. The aerosol enters the oven after passing through the CS maintained at 320°C. The initial peak seen for the oil samples is the volume concentration upstream of the oven. These volume concentrations are calculated from the volume weighted size distributions plotted in Figure 19. John Deere (JD) lube oil has the highest volume concentration upstream of the oven. 100A (Ca/P/S) and 102A (Ca/S) have a similar profile of volume concentration. Oil 103A (Mg/B) shows a mode at 20 nm as compared to 100A and 102A which show a mode at 40 nm. 101A (Zn/S/P) had the lowest volume concentration.

Table 5 shows volume concentrations leaving the CS (upstream) and the oven (downstream) and the fraction surviving passage through the oven for the different lube oil blends.

The JD oil has the highest volume concentration upstream followed by 100A (Ca/P/S), 102A (Ca/S), 103A (Mg/B) and 101A (Zn/S/P). The upstream concentration is a measure of the amount material not volatilized and removed by the CS at 320°C, not a measure of the ash concentration. The high concentration exhibited by the JD oil suggests the presence of low volatility compounds in the additive package.

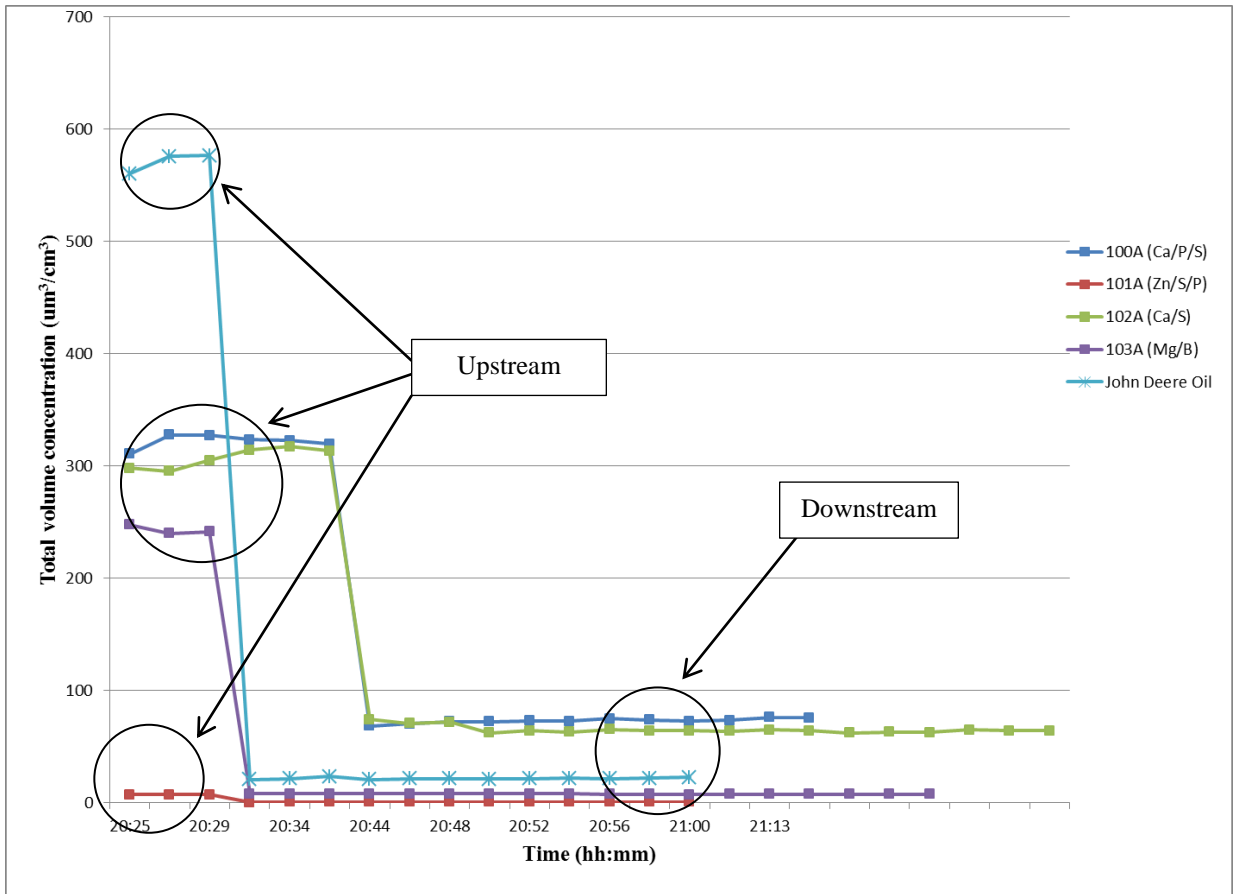


Figure 18: Upstream and downstream number concentration for different blends of lube oil (Upstream concentrations are measured after the CS)

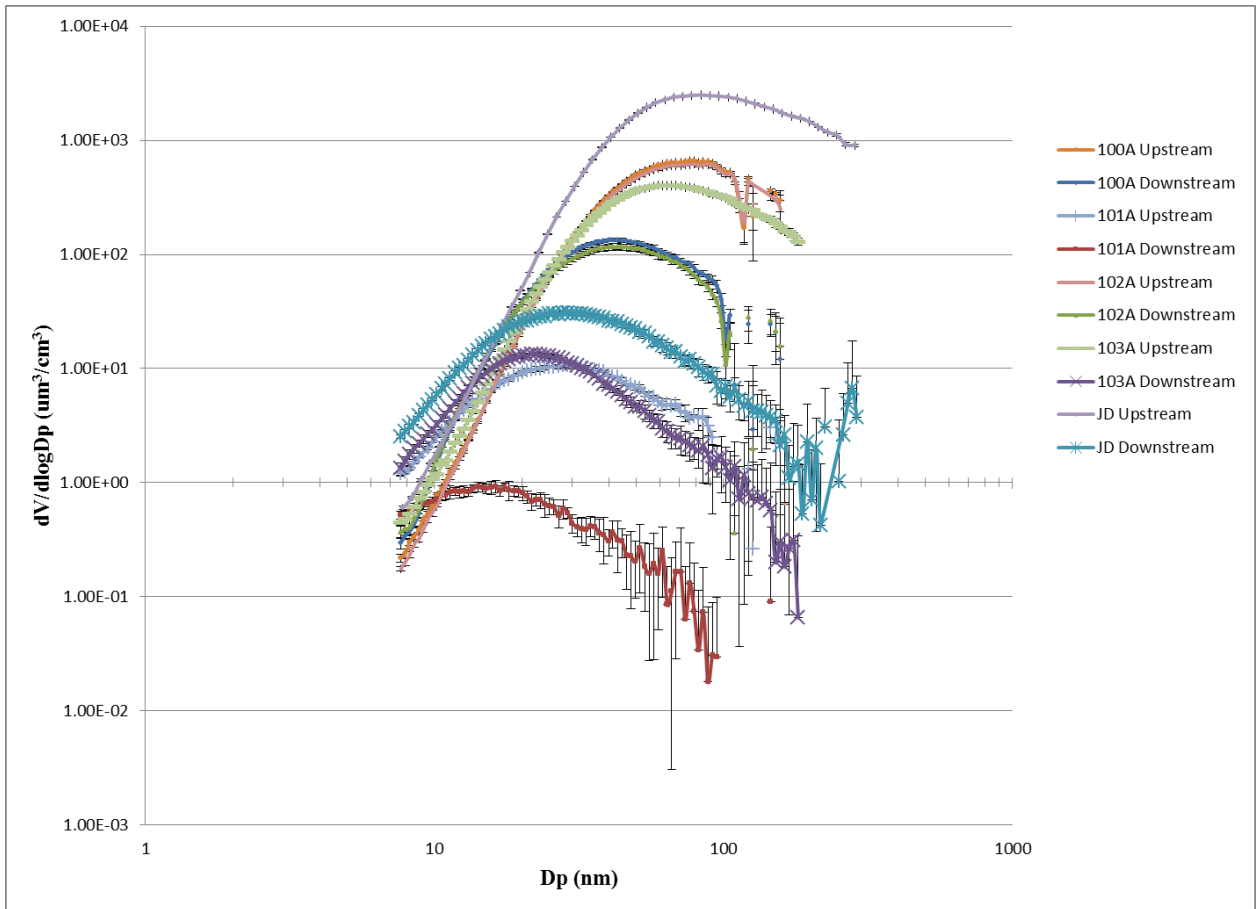


Figure 19: Volume weighted size distributions for different blends of lube oil

Downstream of the oven, lube oil 100A (Ca/P/S) and 102A (Ca/P/S) attain a similar volume concentration of around  $70 \text{ um}^3/\text{cm}^3$ , JD oil stabilizes at  $21.5 \text{ um}^3/\text{cm}^3$ , 103A (Mg/B) stabilizes at  $20 \text{ um}^3/\text{cm}^3$  and 101A (Zn/S/P) has the least volume concentration of  $0.5 \text{ um}^3/\text{cm}^3$ . These concentrations are a measure of the refractory compounds in the oil that survive heating to  $1150^\circ\text{C}$ .



Table 5: Volume fraction for different blends of lube oil

Lube Oil	Upstream Vol. Conc. ( $\mu\text{m}^3/\text{cm}^3$ )	Downstream Vol. Conc. ( $\mu\text{m}^3/\text{cm}^3$ )	Volume Fraction (%)
<b>100A (Ca/P/S)</b>	321.8	72.8	$22.6 \pm 0.6$
<b>101A (Zn/S/P)</b>	7.06	0.55	$7.8 \pm 0.5$
<b>102A (Ca/S)</b>	307.1	65.0	$21.2 \pm 2.0$
<b>103A (Mg/B)</b>	243	7.6	$3.2 \pm 0.2$
<b>John Deere (JD) Oil</b>	570.8	21.5	$3.7 \pm 0.2$

Among the specially blended oils, the ratio of mass of Ca in 100A to the mass of Mg in 103A is 7.9. Downstream of the oven this ratio increases to  $8.9 \pm 0.6$ . This demonstrates that Ca survival is higher. Zinc additized oil (101A) is very volatile and most of it has already evaporated after passing through the CS. Oil 102A contains a very high concentration of sulfur but this seems to have little influence on the concentration leaving the CS and the oven. This is consistent with the EDS measurements, which detected no sulfur.

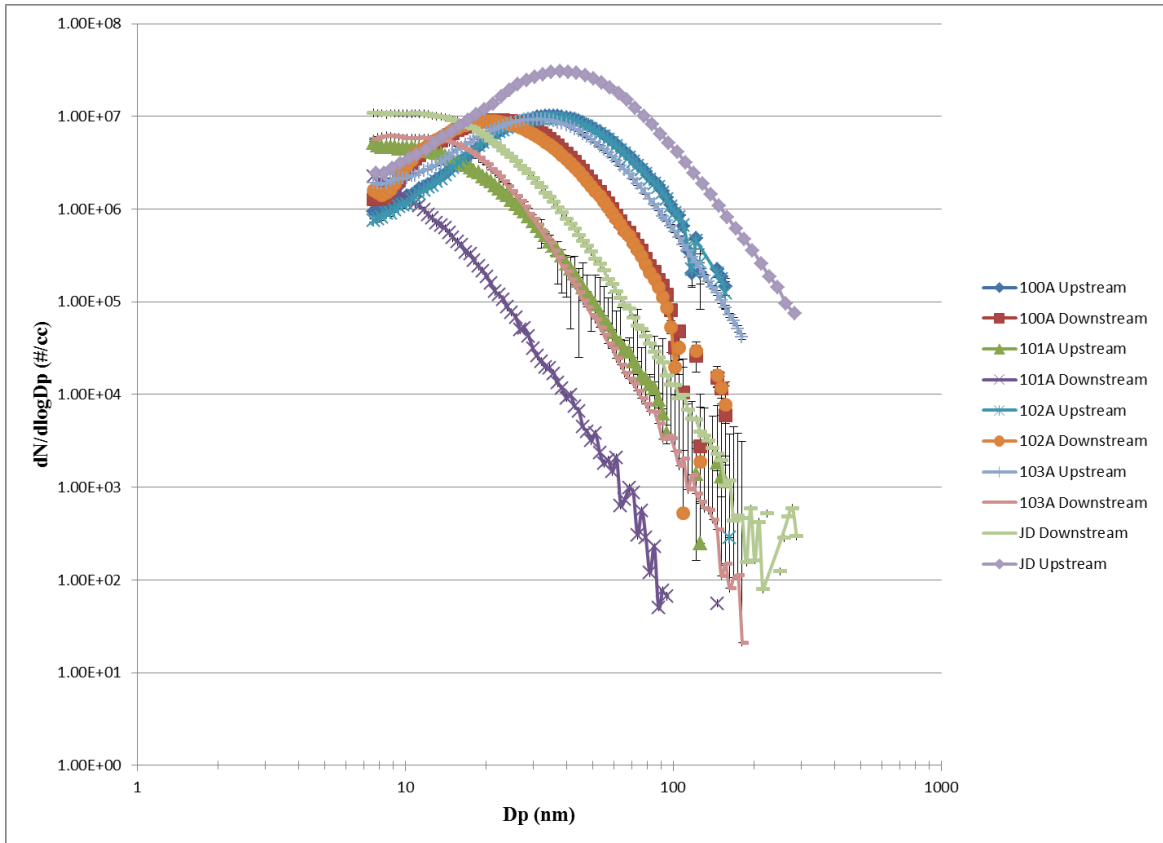


Figure 20: Number weighted size distribution for different blends of lube oil

Figure 20 shows number weighted size distribution for the lube oils. JD Oil has the highest concentration of the particles upstream of the oven. The trends are similar to those seen in the volume distributions.

Figure 21 shows TEM images of two randomly chosen meshes for sample 100A. The dark spots on the picture represent calcium particles. The particles seen are in the range of 5-40 nm which matches well with the size distribution seen in Figure 22 below. Upon heating to 1150°C, the mode shifts from 40 nm to 20 nm.

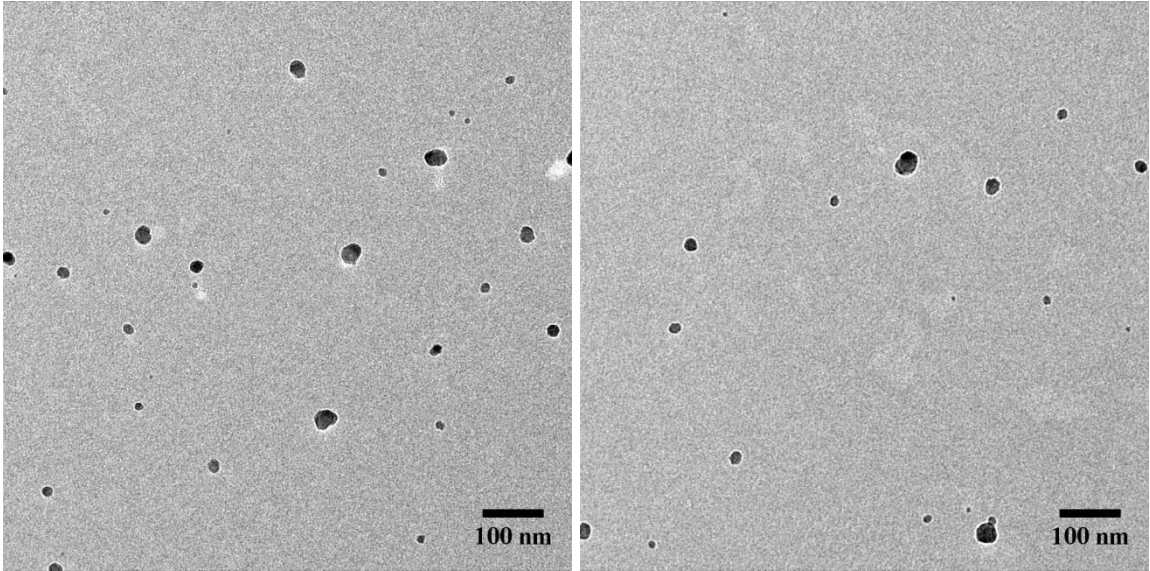


Figure 21: TEM images of sample 100A (Ca/P/S) downstream of the oven

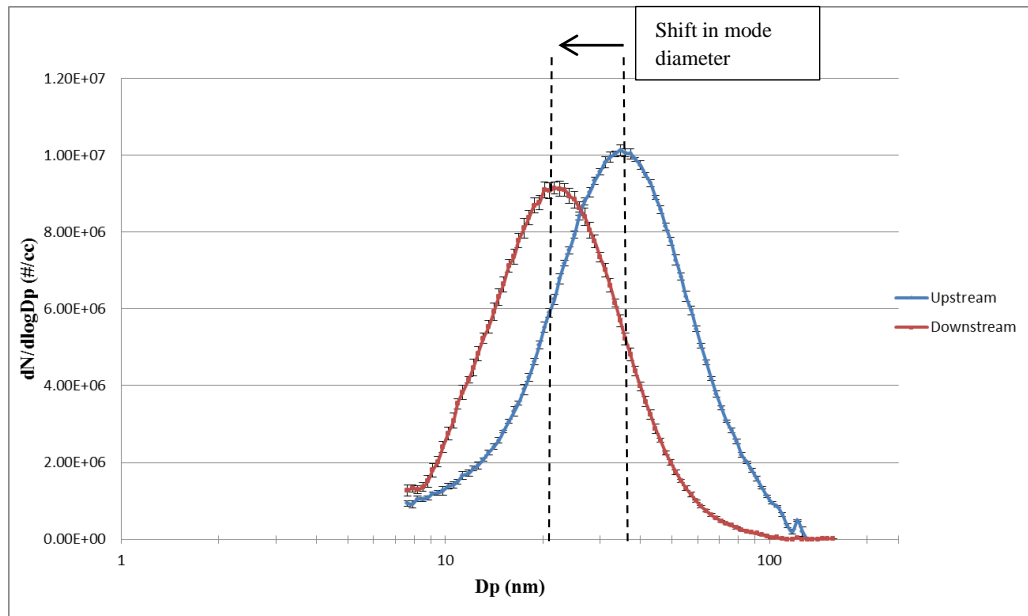


Figure 22: Number weighted size distribution for sample 100A (Ca/P/S)

In Figure 23, TEM images of sample 101A (Zn/S/P) measured downstream of the oven can be seen. The particles are spherical and are in the range 5-20 nm, much smaller than seen with 100A (Ca/P/S). The TEM images are consistent with the number weighted size distributions shown in Figure 24 where downstream of the oven with nearly all particles are smaller than 20 nm. This is also consistent with the small volume fraction reported in Table 5.

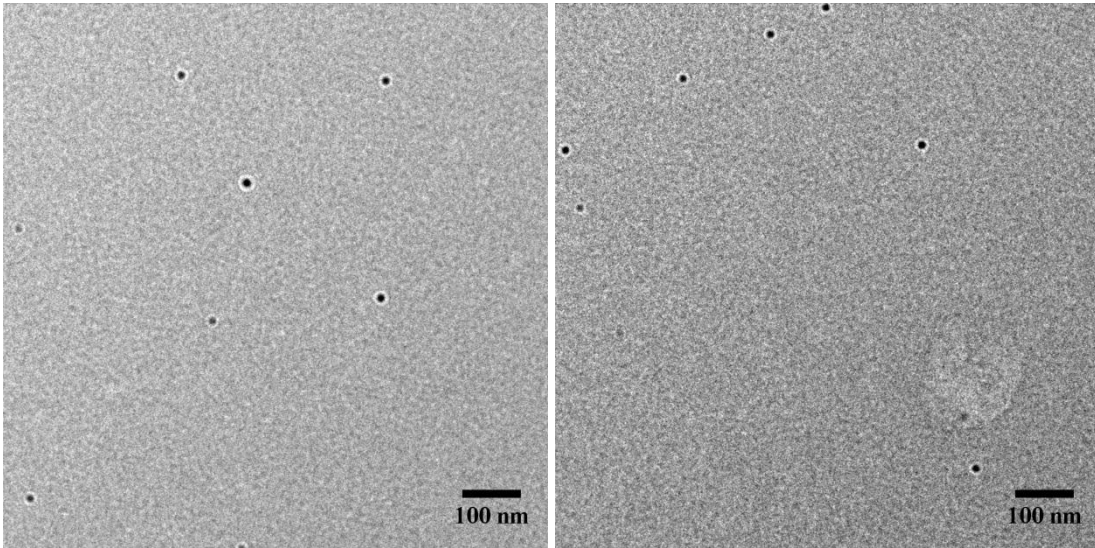


Figure 23: TEM images of sample 101A (Zn/S/P)

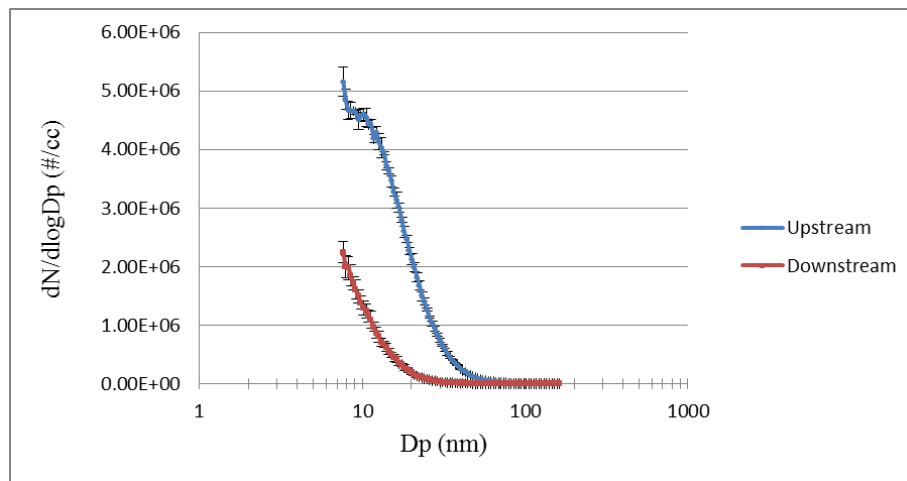


Figure 24: Number weighted size distribution for sample 101A (Zn/S/P)

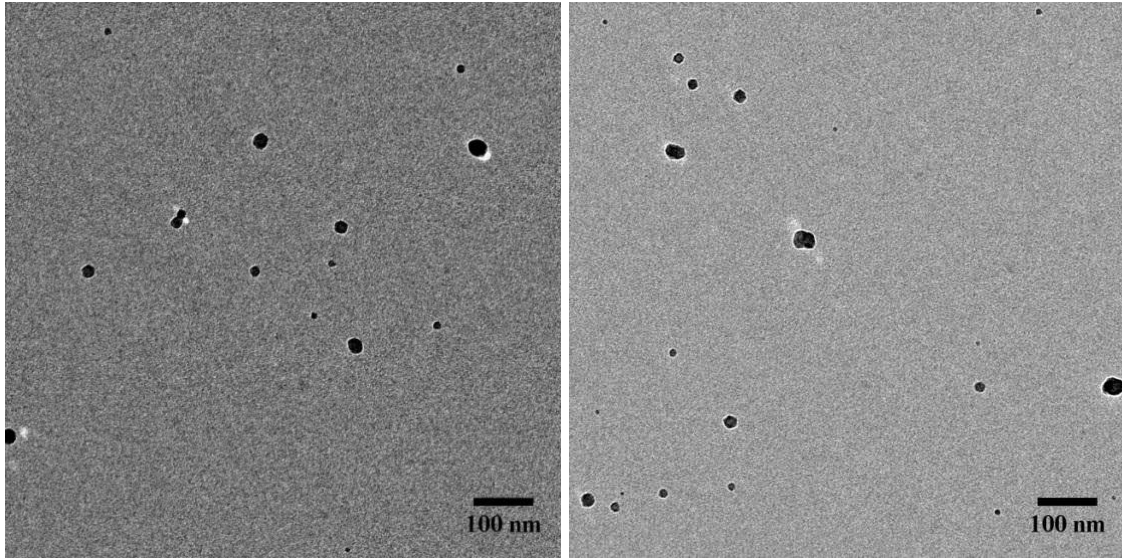


Figure 25: TEM images of sample 102A (Ca/S)

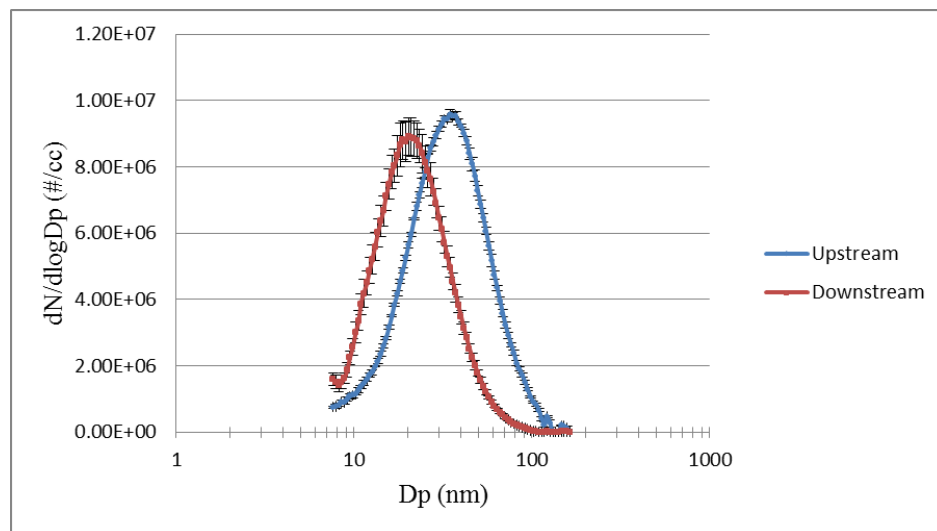


Figure 26: Number weighted size distribution for 102A (Ca/S)

Oil 102A (Ca/S) has a similar Ca concentration to 100A (Ca/P/S) but has a much higher sulfur concentration. However, the sulfur seems to have little influence as it volatilizes in the oven and the TEM images and size distributions shown in

Figure 35 and Figure 36 are similar to those observed with 100A. Energy dispersive spectroscopy (EDS) analysis of the particles shows the presence of calcium but not

sulfur. Particles downstream of the oven are in the size range of 5-40 nm with a mode around 20 nm while upstream of the oven the particles are larger with a mode around 40 nm.

Figure 27 shows TEM images of the particles measured downstream of the oven with oil 103A (Mg/B). Particles deposited on the grid are spherical and are randomly dispersed. The size distributions shown in Figure 28 show that the mode shifts from about 40 nm to below 15 nm on heating. The downstream distribution shows most of the particles below 40 nm in general agreement with the TEM images.

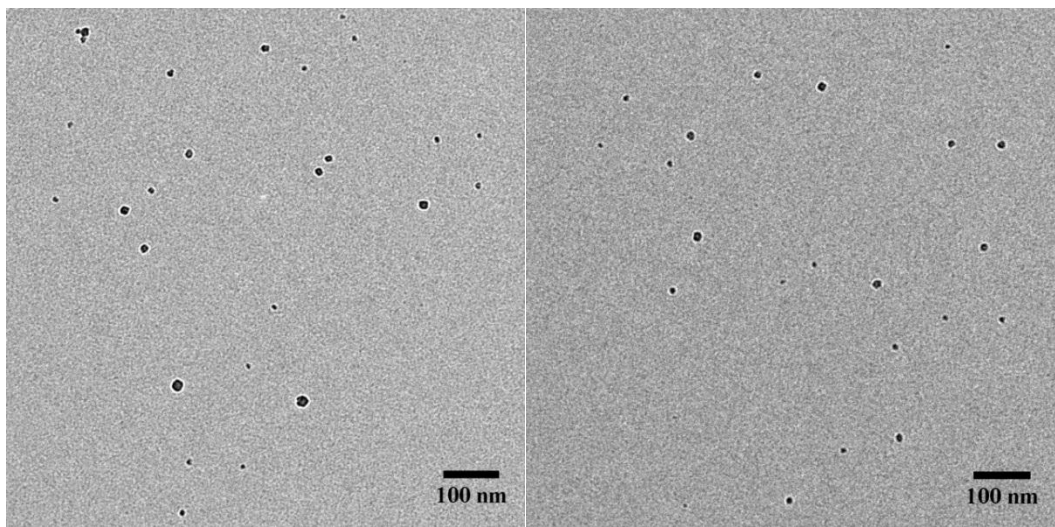


Figure 27: TEM images of sample 103A (Mg/B)

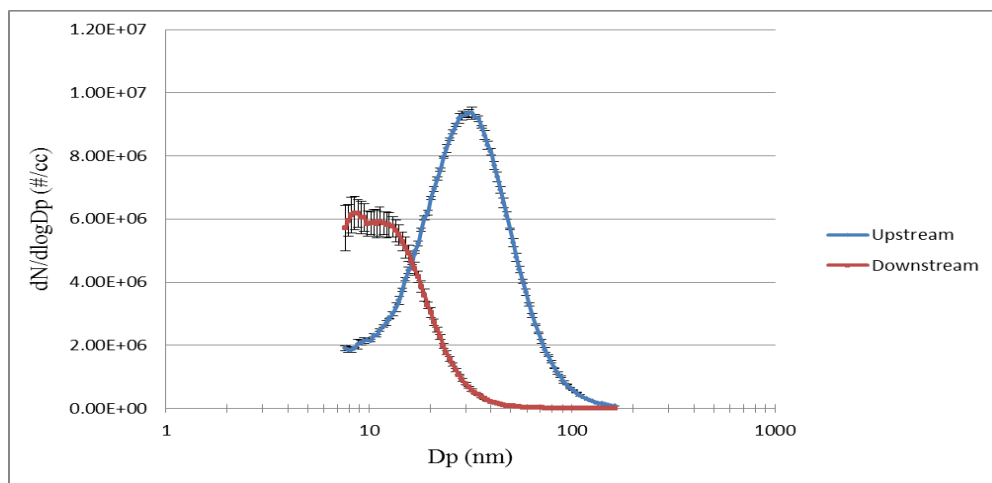


Figure 28: Number weighted size distribution for sample 103A (Mg/B)

Figure 29 shows TEM images for John Deere Oil. The particles are spherical in shape and randomly dispersed. Due to low particle concentration on the mesh, EDS analysis was performed by focusing on a group of particles as seen in Figure 30. The elemental composition of particles showed the presence of Ca, Mg as seen in Figure 30.

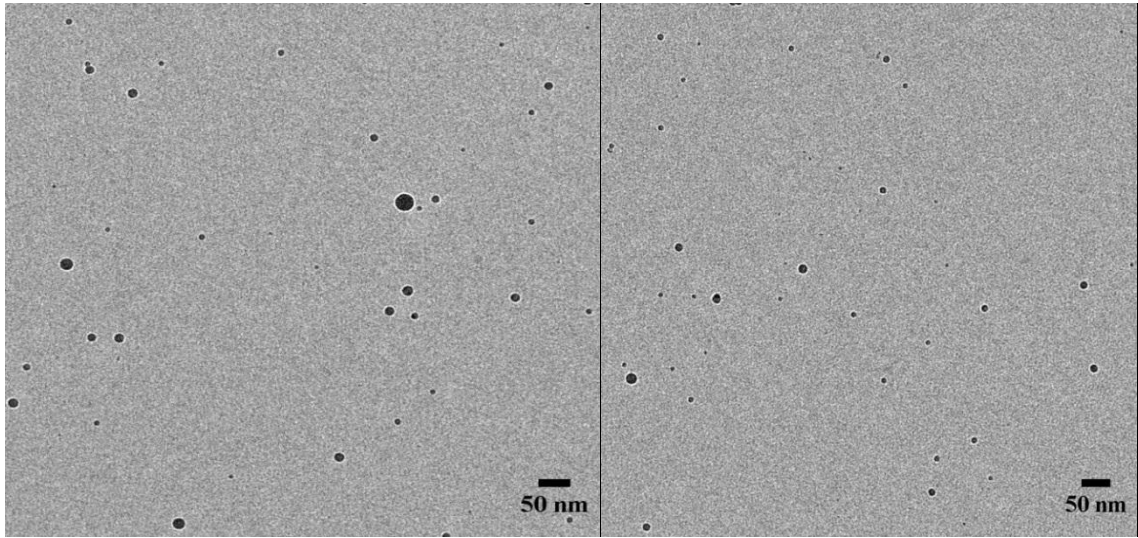


Figure 29: TEM images of John Deere lube oil

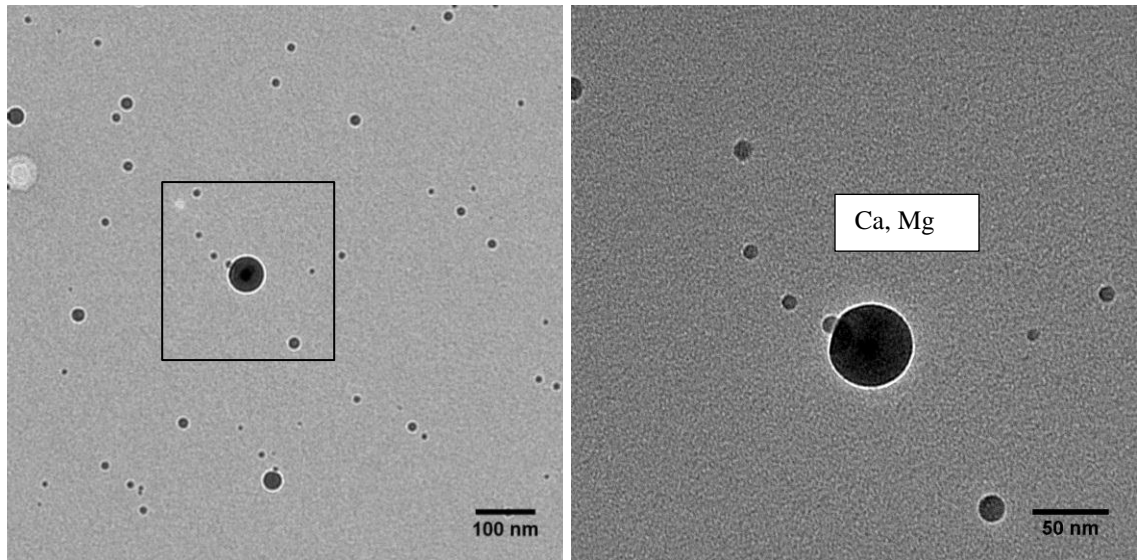


Figure 30: EDS analysis of the particle (on the right) showed the presence of Ca and Mg

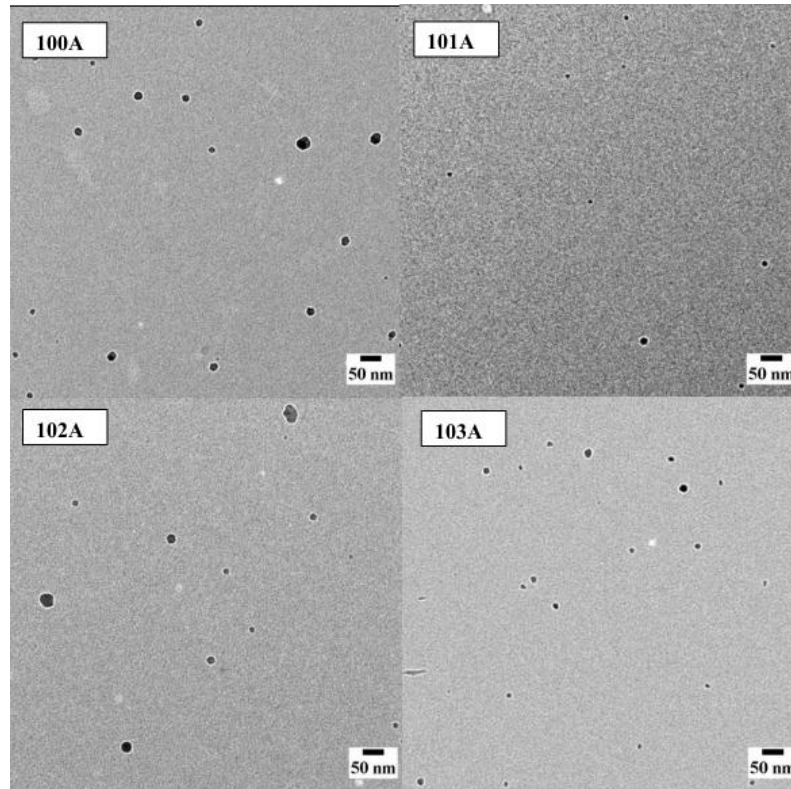


Figure 31: Comparison of TEM images between different lube oils

From Figure 31, it can be seen that lube oil 100A (Ca/P/S) and 102A (Ca/S) have similar particle morphology and diameter range of 5-40 nm. EDS analysis of sample 100A (Ca/P/S) and 102A (Ca/S) showed the presence of calcium. The particles formed for 100A (Ca/P/S) and 102A (Ca/S) are likely calcium oxide particles as it is the only calcium compound which is stable at a temperature of 1150°C and chemical equilibrium model discussed by Gladis (2010) suggests its formation.

For lube oil 101A (Zn/S/P), the particles deposited on the grid are smaller, spherical, and in the range of 5-20 nm. The smaller survival fractions and particles produced by the zinc additized oil compared to the calcium and magnesium additized oils could be due to low temperature dissociation of ZDDP. The magnesium additized oil 103A (Mg/B) shows particle size in the range of 5-30 nm. EDS analysis of 101A (Zn/S/P) and 103A (Mg/B) did not yield any results as the mass concentration on the grids was below the detectability limits of the EDS.



## 4.2: Calibration experiment with aqueous salt sprays

The primary objective of the aqueous salt calibration experiments is to estimate the survival fraction for different metallic compounds present in engine exhaust ash as they pass through the HTOM system. The metallic compounds found in ash are due to additives used in the lube oil to enhance its properties. Wear metals and metals present in the fuel either as additives or contamination may also contribute but the focus of this work is ash resulting from engine oil additives. The most common additive metals are calcium, zinc, and magnesium. They are converted in the engine to metallic sulfates and phosphates which are the primary compounds found in ash (Takeuchi et al., 2003, Givens et al. 2003). For this experiment study, salts of calcium, magnesium and zinc were examined.

A preliminary experiment was run without the CS in the system continuously ramping the temperature from ambient, 25°C to 1150°C to determine the temperature at which the particles started to change. A zinc sulfate aerosol was used for these experiments and a TSI EEPS, a fast response sizing instrument was used to measure the size distribution downstream of the oven. The lube oil spray experiments showed very poor survival of particles from the zinc additized oil but other work has shown that zinc compounds, mainly zinc phosphate are found in engine exhaust ash (Sappok, Rodrick & Wong ,2010). Thus, it is important to understand the fate of zinc compounds as they pass through the oven. Zinc phosphate is nearly insoluble and tests done with it gave poor repeatability. Consequently zinc sulfate hexahydrate was used in this test because it is soluble and gave repeatable results. Figure 32 is a plot of the volume concentration against temperature corrected for thermophoretic loss. Thermogravimetric (TGA) analysis of zinc sulfate hexahydrate shows that it loses five water molecules below 100°C and the remaining one by about 250°C. The resulting anhydrous zinc sulfate should be stable until about 650°C when it decomposes to form zinc oxide (Mu and Perlmutter, 1981). Chemical equilibrium calculations by Gladis (2010) suggest that zinc sulfate starts to decompose at 700°C. Figure 32 shows an initial loss of volume between 50°C and 150°C a subsequent drop between about 250°C and 300°C and apparent subsequent decomposition starting around

500°C. Thus the pattern is the same as predicted by TGA analysis but the temperatures are shifted somewhat. This is not surprising because in TGA a bulk sample is heated and mass determined as a function of temperature. The thermodynamic calculations are based on bulk phase properties as well. In the experiment done here the material is in the form of nanoparticles and the loss of volume is monitored. In any case, the corrected volume is nearly constant in the range of 300-350°C and this should correspond to dry anhydrous zinc sulfate.

The other salts sprayed are more stable than zinc sulfate and are assumed to be fully dried and in anhydrous form at the CS outlet temperature of 320°C. Zinc phosphate hydrate loses water in three stages between 80°C and 370°C and melts at 900°C (Boonchom, 2010). Anhydrous magnesium sulfate melts at 1137°C (handbook of chemistry and physics) and anhydrous calcium sulfate melts at 1460°C (handbook of chemistry and physics). The CS was kept in the system for all of the experiments described here to insure a dry stable aerosol entering the oven.

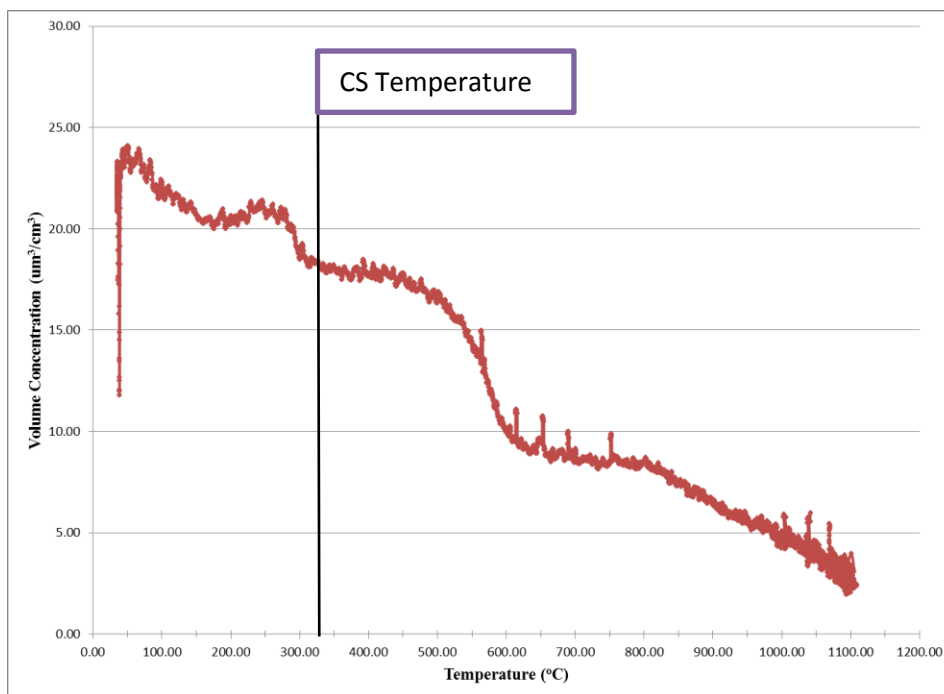


Figure 32: Volume concentration of ZnSO<sub>4</sub> as a function of temperature

#### 4.2.1 Zinc sulfate penetration results

In these experiments particle size distributions were measured with the SMPS at three temperatures, upstream of the oven but after the CS where the aerosol was dried and conditioned at 320°C, and then cooked to ambient temperature; 800°C; and 1150°C. Technical grade zinc sulfate hexahydrate was used for this study. Volume weighted size distributions are shown in

Figure 33. The upstream condition is the CS outlet which is at ambient temperature. Heated particles shrink and lose volume as a result of water loss, decomposition, phase transformation, and evaporation. Figure 34 is a plot of volume fraction against oven temperature. Volume fraction is the ratio of the total particle volume at the given oven temperature to the total particle volume at the inlet temperature - ambient. The volume fraction of zinc sulfate drops with increasing temperature decreasing to 43% and 7% at temperatures of 800°C and 1150°C, respectively. This is similar to the results of the lube oil spray experiments with the zinc containing oil which showed 7.8% survival when heated from the CS outlet temperature to 1150°C suggesting that the particles leaving the CS in the lube oil spray experiment may have been zinc sulfate, which has a melting point of 680°C

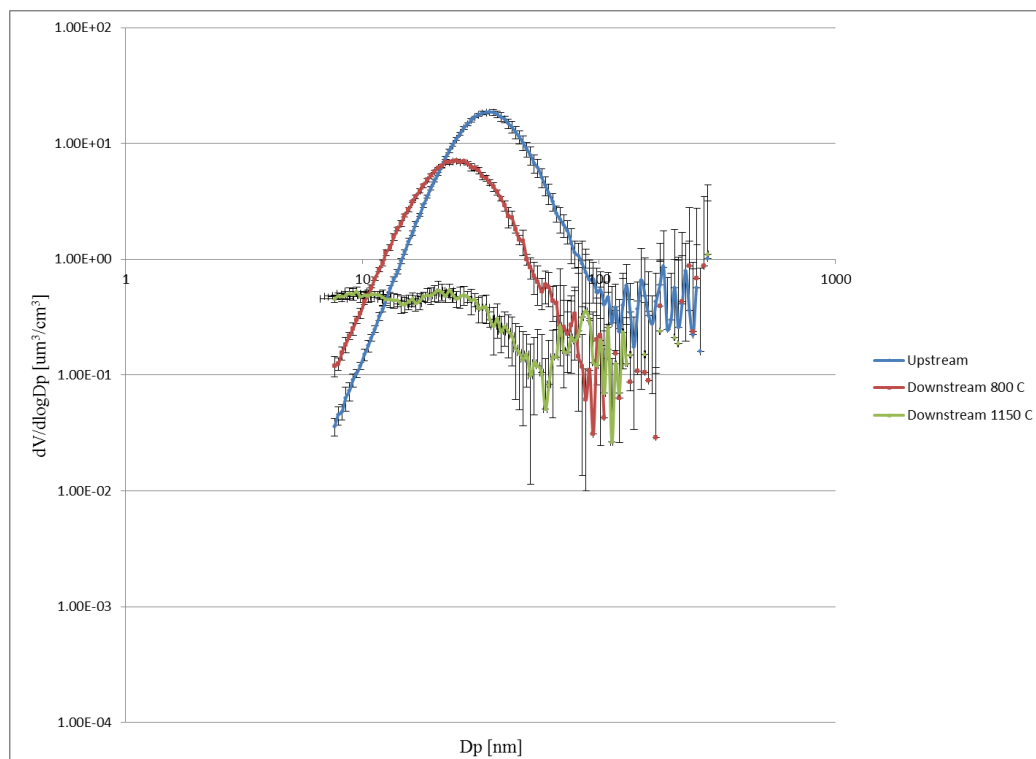


Figure 33: Volume weighted size distribution for zinc sulfate at 25°C, 800°C and 1150°C (Upstream concentration is measured after the CS)

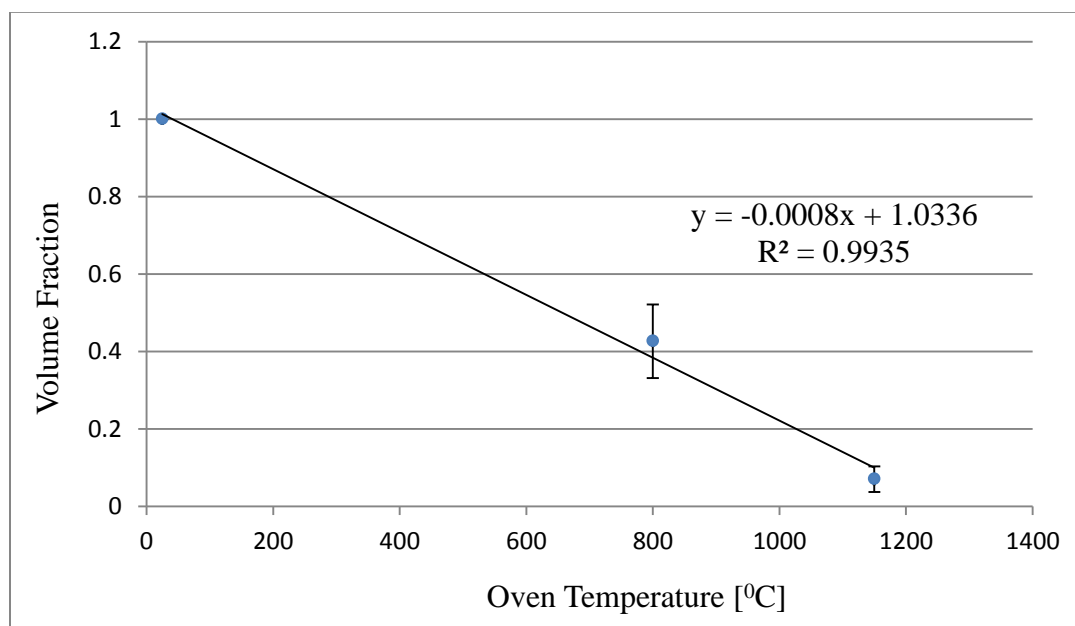


Figure 34: Volume fraction vs temperature for zinc sulfate

#### 4.2.2 Zinc phosphate penetration results

ZDDP is used as an anti-wear additive in diesel engine oils. It is a complex compound consisting of zinc, phosphorus and sulfur compounds. Studies done on oil containing only ZDDP additives showed that it produced ash primarily containing  $Zn_3(PO_4)_2$  and  $Zn_2P_2O_7$  (Sappok, Rodriguez and Wong, 2010).

Figure 35 shows volume weighted size distributions for zinc phosphate aerosols at three temperatures. Like the zinc sulfate aerosol, particles shrink and the volume decreases at higher temperatures. The size distributions are quite irregular and the upstream condition has a clear bimodal structure. This may be due to problems associated with the insolubility of zinc phosphate.

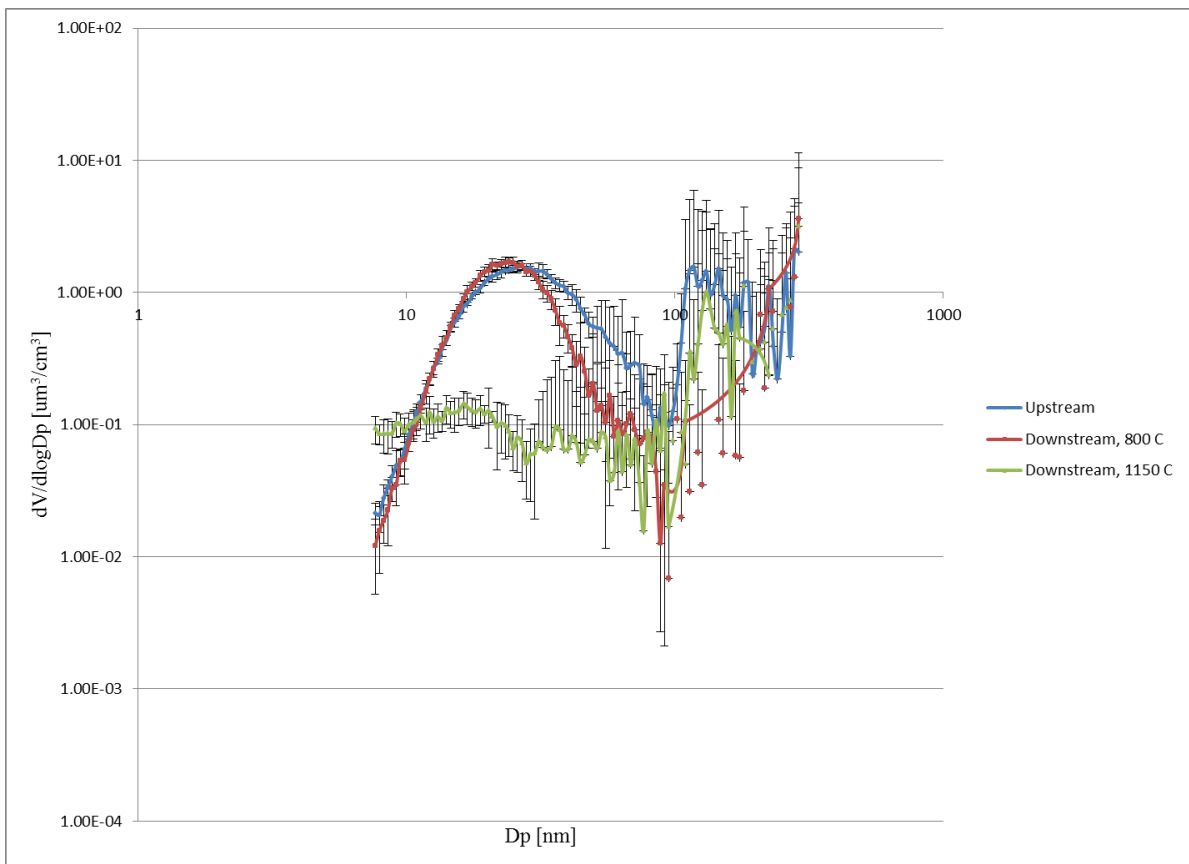


Figure 35: Volume weighted size distributions for zinc phosphate(Upstream concentration is measured after the CS)

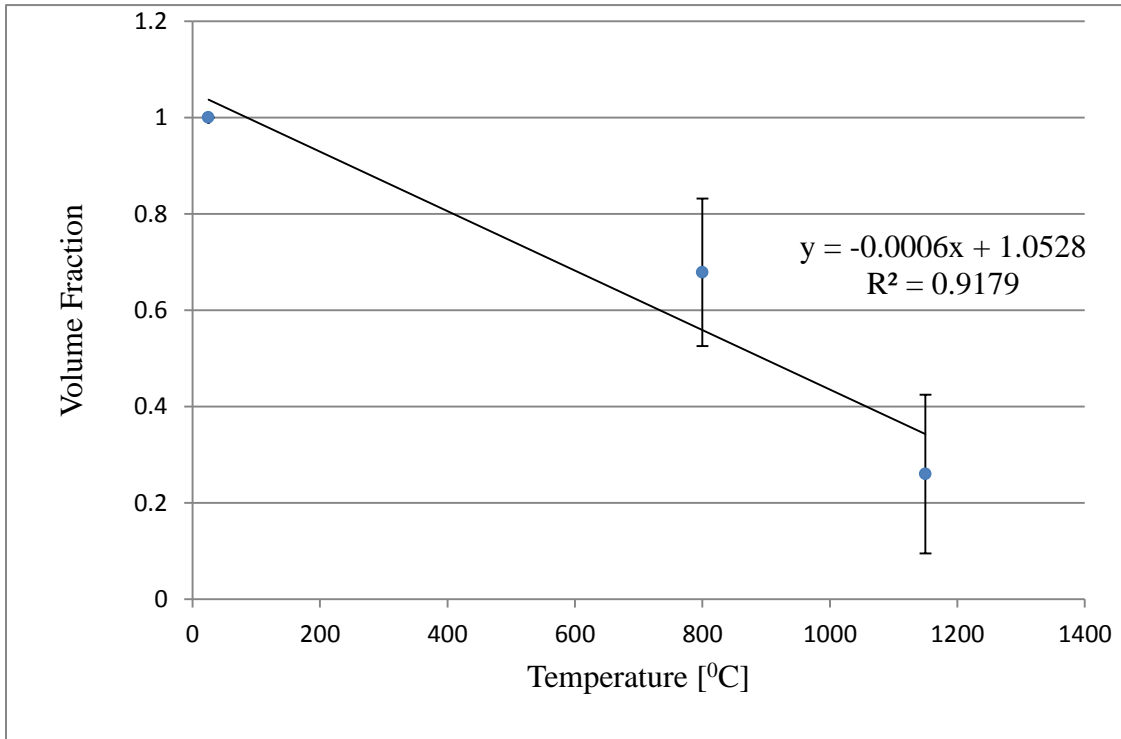


Figure 36: Volume fraction vs temperature of zinc phosphate

Figure 36 is a plot of zinc phosphate volume fraction against temperature. The volume fractions are 68% and 26% at temperatures of 800°C and 1150°C, respectively. Zinc phosphate has a melting point of 900°C. Compared to zinc sulfate, zinc phosphate had a higher volume fractions surviving. However, zinc phosphate was less repeatable as compared to zinc sulfate and had higher standard deviation at 800°C and 1150°C. The insolubility of zinc phosphate made it difficult to make consistent spray solutions. TEM analysis was done for zinc phosphate spray to check if the particles produced were zinc phosphate. It showed that the particles were made of zinc and phosphorus. The results of the TEM EDS analysis are given in appendix IV.

### 4.2.3 Magnesium sulfate penetration results

Previous studies done on commercially available SAE-40 oil showed that the ash was composed of primarily contained calcium sulfate ( $\text{CaSO}_4$ ) and zinc magnesium phosphate ( $\text{Zn}_2\text{Mg}(\text{PO}_4)_2$ ) (Sappok, Rodriguez and Wong, 2010) but magnesium sulfate  $\text{MgSO}_4$  was not observed.

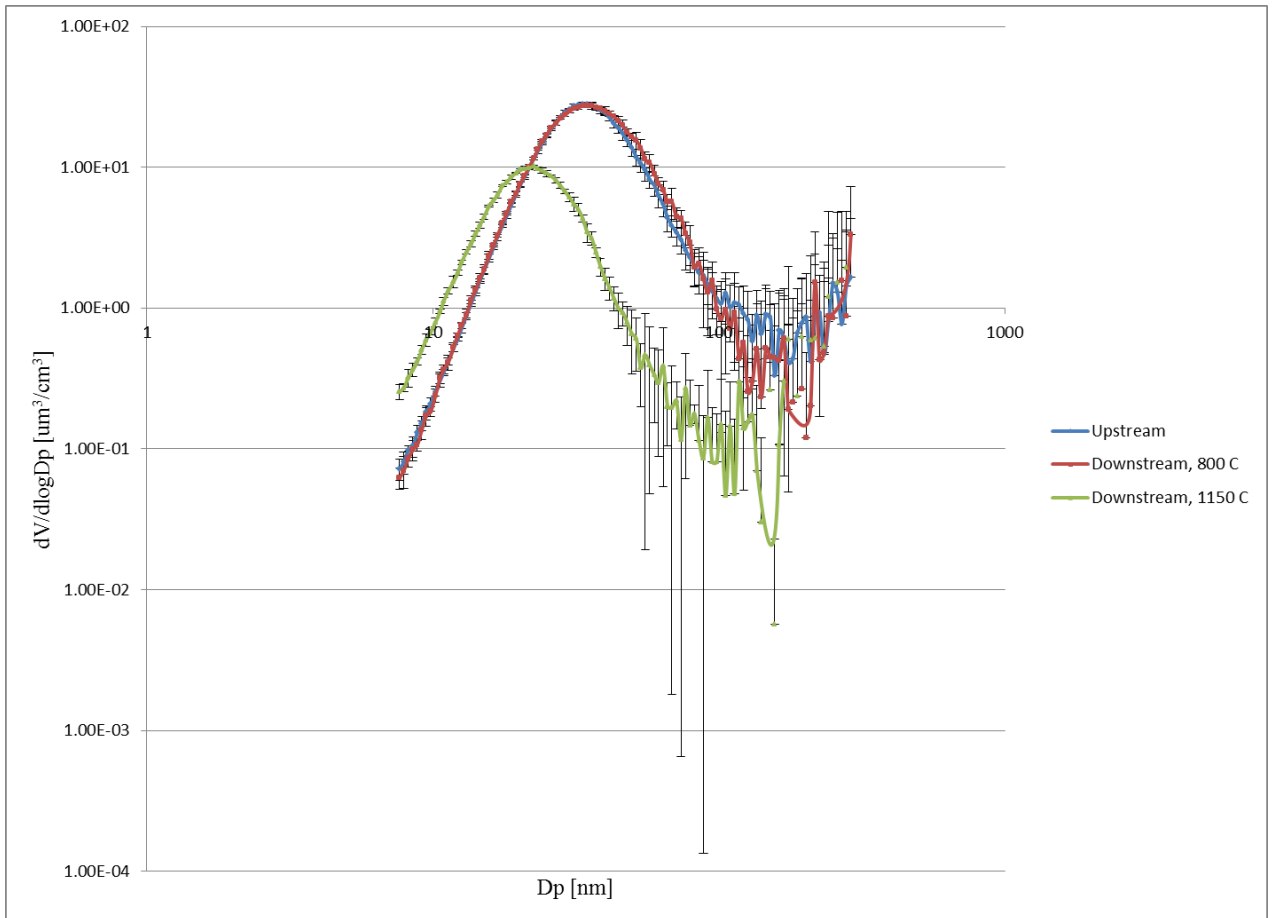


Figure 37: Volume weighted size distributions for magnesium sulfate (Upstream concentration is measured after the CS)

Figure 37 shows volume weighted size distributions for magnesium sulfate sprays at the three temperatures. At 800°C, there is no change in volume concentration demonstrating

the stability of magnesium sulfate particles. However, at 1150°C, there is a shift in the size distribution towards smaller particles as the particles volatilize as they are heated past the melting point of magnesium sulfate which is 1137°C.

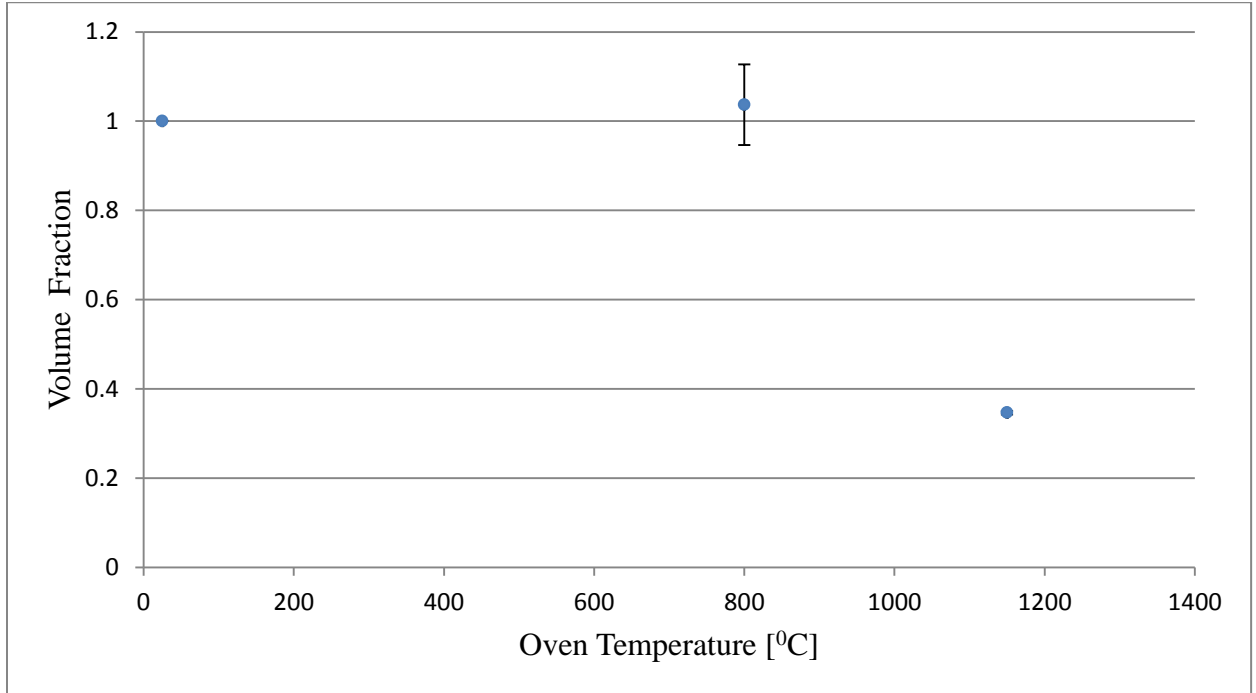


Figure 38: Volume fraction vs temperature for magnesium sulfate

As seen in Figure 38, at 800°C, the volumetric fraction has a value slightly greater than expected due to overcorrection of thermophoretic losses. Since there is no substantial decrease in the volume fraction at 800°C, it indicates that magnesium sulfate is stable at 800°C. As the temperature is ramped up to 1150°C, the volumetric fraction of magnesium sulfate reduces to 35%. The error bars are too small to be seen at 1150°C showing it is very stable at 1150°C.



#### 4.2.4 Calcium sulfate penetration results

Calcium sulfate is observed to be the predominant lubricant derived component found in ash, with concentrations ranging from 59%-75% of the total ash (Barris, Reinhart and Wahlquist, 1991, Nemoto et al., 2004, McGeehan et al., 2005). The difference in the reported values demonstrates the underlying need to understand the behavior of calcium sulfate in greater detail.

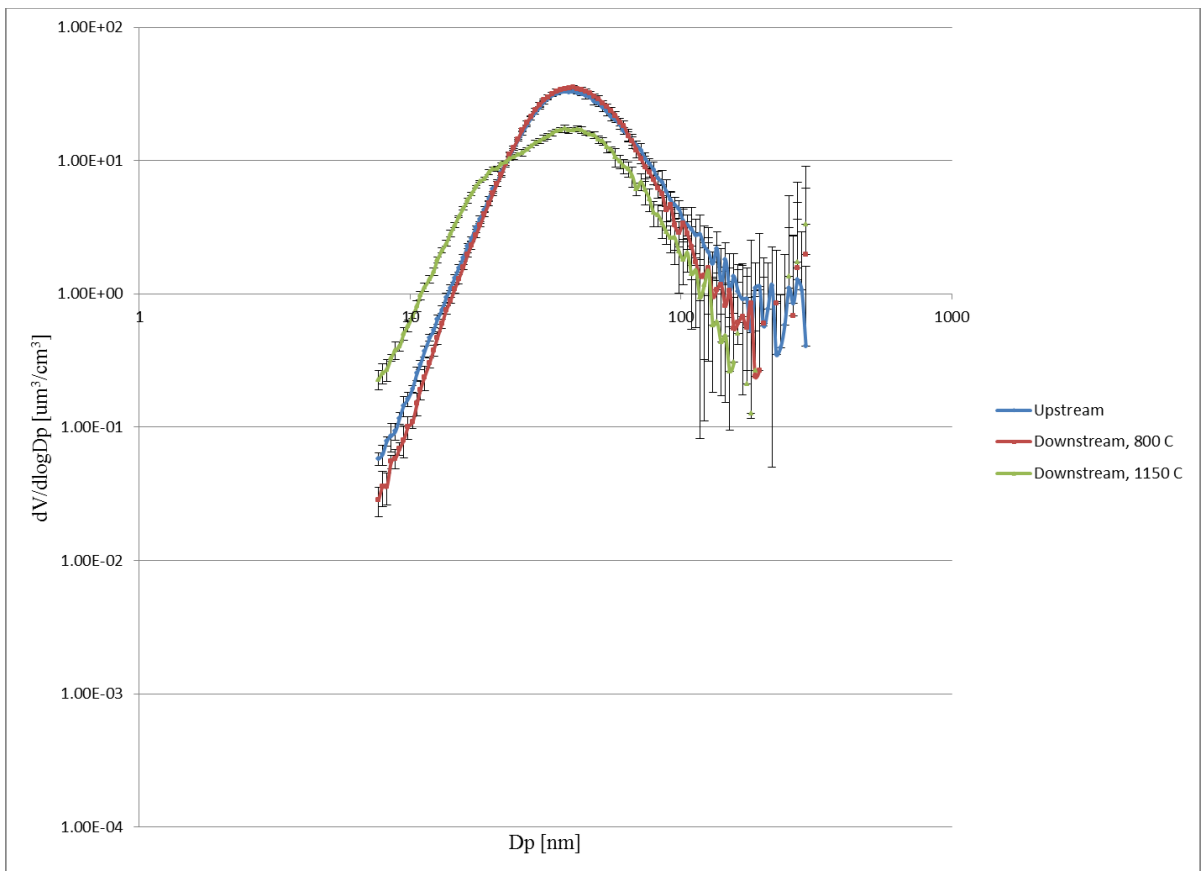


Figure 39: Volume weighted size distributions for calcium sulfate (Upstream concentration is measured after the CS)

In Figure 39, volume weighted size distribution is shown. At 800°C, the size distribution doesn't show any change in distribution similar to MgSO<sub>4</sub> particles. However at 1150°C, the particles shrink causing a decrease in volume concentrations.

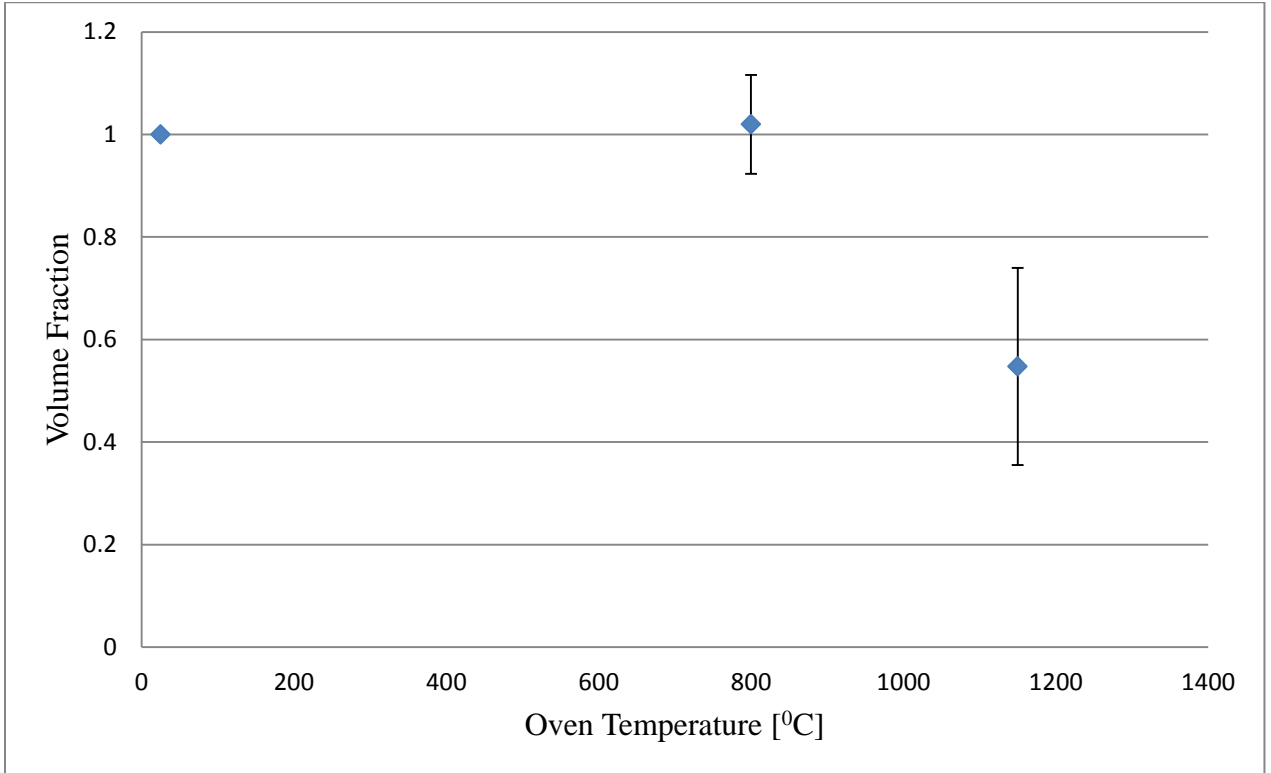


Figure 40: Volume fraction vs Temperature for Calcium Sulfate

The volume fraction of calcium sulfate at three different temperatures is shown in Figure 40. CaSO<sub>4</sub> has a melting temperature of 1460°C. At 800°C, it has a volume fraction of  $1.0 \pm 0.1$ , similar to MgSO<sub>4</sub> particles. At 1150°C, the penetration of calcium sulfate drops to 55%. This is higher than for the other metal salts sprayed and is consistent with the high melting point.

Results from the aqueous salt spray experiments form the basis for predicting the penetration for likely ash constituents. Table 6 summarizes the results for the salt study.

Table 6: Summary of volumetric fraction survival at different temperatures

<b>Salt</b>	<b>Volumetric fraction at 800<sup>o</sup> C (%)</b>	<b>Volumetric fraction at 1150<sup>o</sup> C (%)</b>	<b>Percentage reduction in volume from 800<sup>o</sup> C to 1150<sup>o</sup> C (%)</b>	<b>Melting Point (Celsius) (Anhydrous)</b>
Zinc sulfate	42.6 ± 9.5	7.1 ± 3.31	83	680
Zinc phosphate	67.8 ± 15.3	25.9 ± 16.5	62	900
Magnesium sulfate	103.6 ± 9.0	34.6 ± 0.3	65	1124
Calcium sulfate	102.6 ± 9.6	54.7 ± 19.2	45	1460

### 4.3 Engine ash experiment

The primary objective of the engine ash experiment is to understand the morphology and chemical composition of the ash formed when engine exhaust particles pass through the high temperature oven. The secondary objective is to predict calcium emissions in real time as calcium is the only element stable enough to be found in measurable concentrations downstream of the oven. Testing was done under steady state engine conditions at 1400 rpm and 250 N-m torque. The experiment was repeated three times and each time, the TEM grid was exposed to the aerosol flow for a period of 4 hours and 20 minutes. The lubricating oil used was John Deere Plus 50 II. The oven was maintained at a temperature of 1150<sup>0</sup>C. The details of the setup and procedure are given in section 3.2.

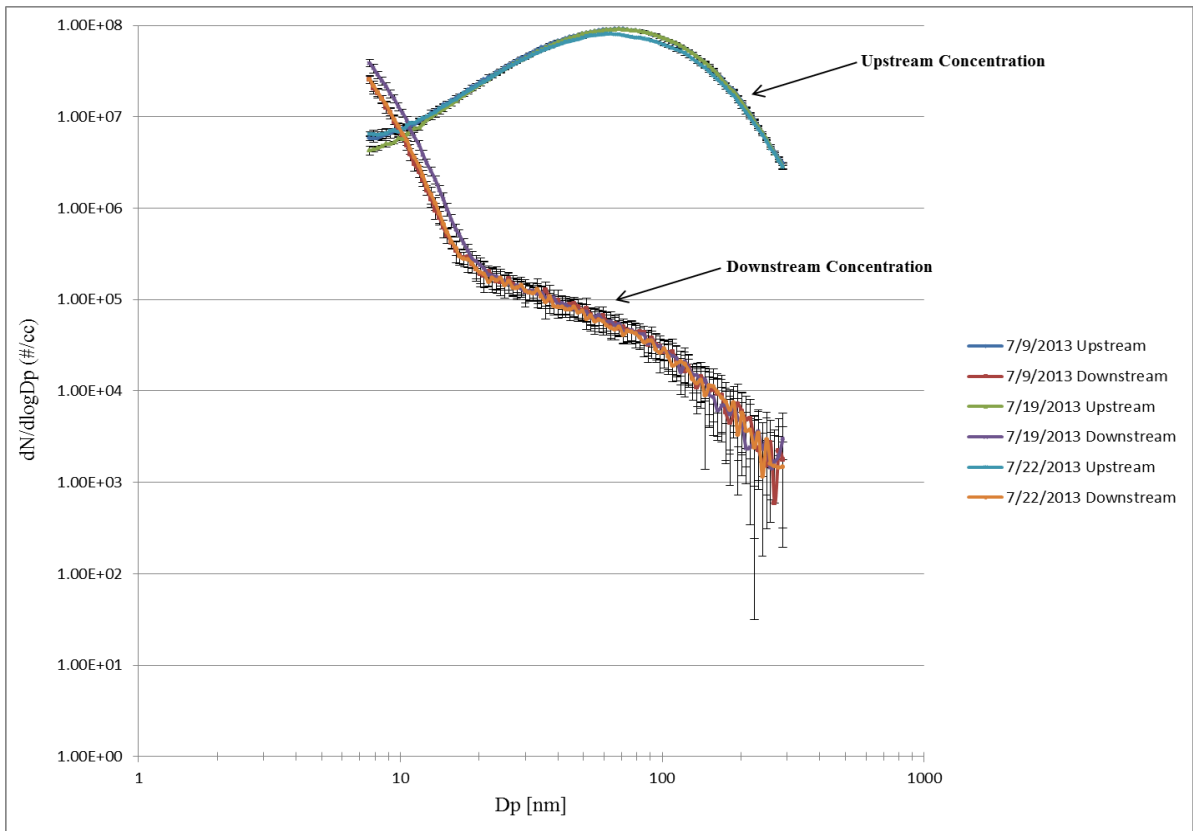


Figure 41: Number weighted size distribution at 250 N-m and 1400 RPM

Figure 41 is a plot of the number weighted size distributions measured upstream and downstream of the oven. The repeats were performed on three different days and are plotted individually in Figure 41. The error bars shown are based on standard deviation of at least three SMPS scans. All concentrations are corrected for thermophoretic losses. The average reduction in total number concentration going through the oven is  $95.2\% \pm 1.3\%$ . The size distribution upstream of the oven is clearly unimodal but downstream of the oven two modes appear. The smaller mode, consisting of particles smaller than about 20 nm is likely associated with ash particles that decorated soot particles where the carbon was oxidized in the oven. The shape of the mode suggests that there are many particles smaller than 8 nm, the lower sizing limit of the SMPS. The origin of the larger mode, consisting of particles larger than about 20 nm is less clear. Two possible explanations come to mind. The first is that some small fraction of the soot particles, less than 1 in  $10^3$  survive oxidation without significant change in size, while the remainder are consumed leaving only as ash residue. Another explanation might be that the mode consists of particles that were originally larger than the upper size limit of the SMPS and are partially oxidized shrinking into the size range of the SMPS.

Figure 42 show the volume weighted size distribution corresponding to the results plotted in Figure 41. Again there is a clear bimodal structure in the aerosols measured downstream of the oven.

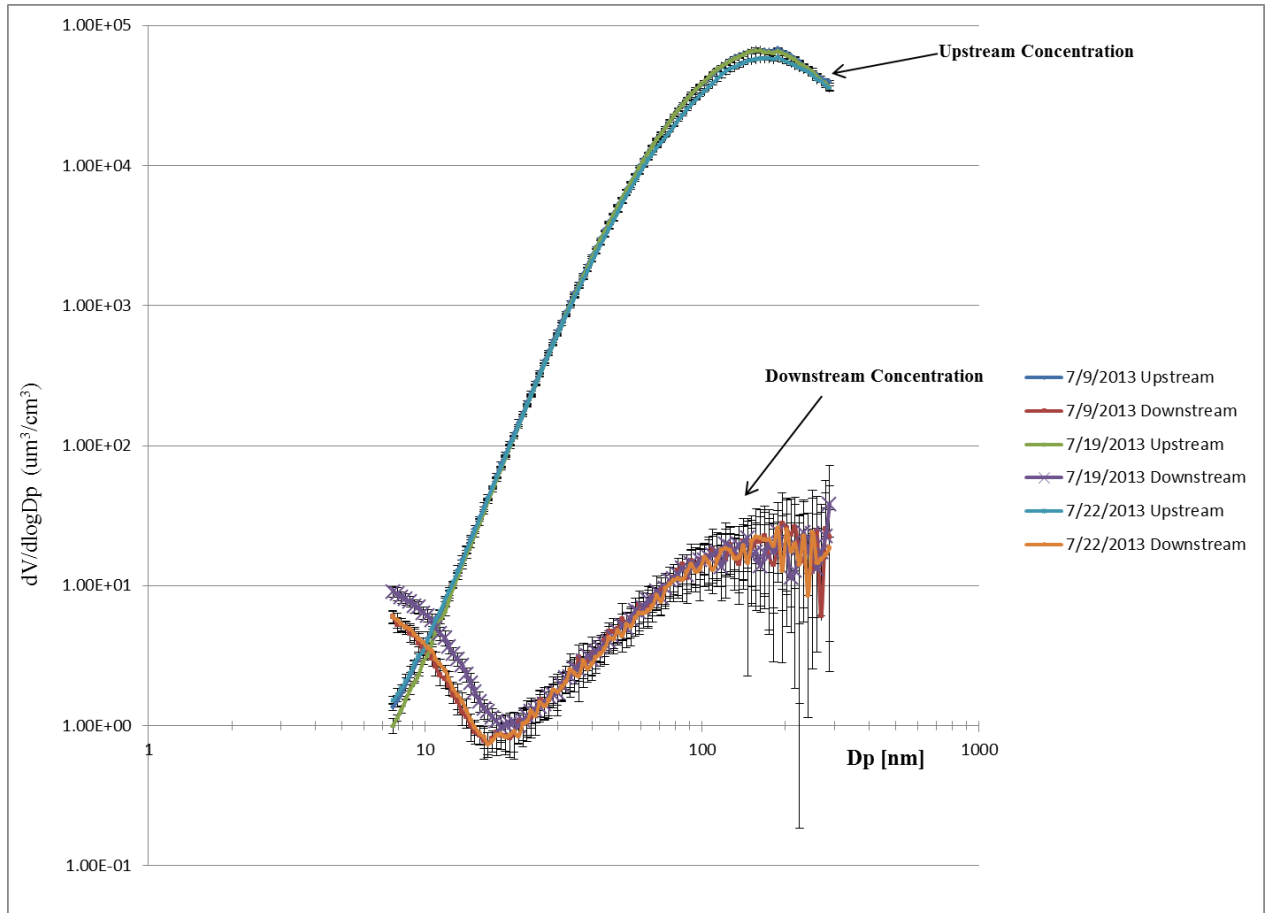


Figure 42: Volume weighted size distribution at 250 N-m at 1400 RPM

Due to particle shrinkage, the volume reduction is much larger than the number reduction, with the volume fraction surviving downstream to be  $4.5 \times 10^{-4}$ . The summary of volume and mass concentration is summarized in Table 7.

Table 7: Summary for mass and volume concentrations

<b>Test Date</b>	<b>Volume Upstream (<math>\mu\text{m}^3/\text{cm}^3</math>)</b>	<b>Volume Downstream (<math>\mu\text{m}^3/\text{cm}^3</math>)</b>	<b>Mass Upstream (<math>\mu\text{g}/\text{m}^3</math>)</b>	<b>Mass Downstream (<math>\mu\text{g}/\text{m}^3</math>)</b>	<b>Mass of ash Upstream (<math>\mu\text{g}/\text{m}^3</math>)</b>
7/09/2013	$3.1 \times 10^5$	13.2	$1.9 \times 10^4$	44.4	56.3
7/19/2013	$3.0 \times 10^5$	13.7	$1.9 \times 10^4$	45.8	58.0
7/22/2013	$2.8 \times 10^5$	12.8	$1.7 \times 10^4$	42.8	54.2
Average	$2.9 \times 10^5 \pm 1937.7$	$13.2 \pm 0.5$	$1.8 \times 10^4 \pm 1254.2$	$44.3 \pm 1.5$	$56.1 \pm 20.07$

If it is assumed that the particles upstream are soot particles with a density distribution given by Park et al. (2003) and the downstream particles are CaO with a density of  $3.35 \text{ g}/\text{cm}^3$ , the indicated mass fraction ash comes out to be  $0.3\% \pm 0.1\%$  which is similar to the reported values in literature

Figure 43 shows TEM images particle samples collected downstream of the oven with the thermal precipitator. The particles observed are in the range of 5-80 nm and are randomly distributed. They are in the same size range as indicated by the SMPS. Some of the particles look like small soot aggregates and likely are contributors to the larger particle mode found in the SMPS analysis.

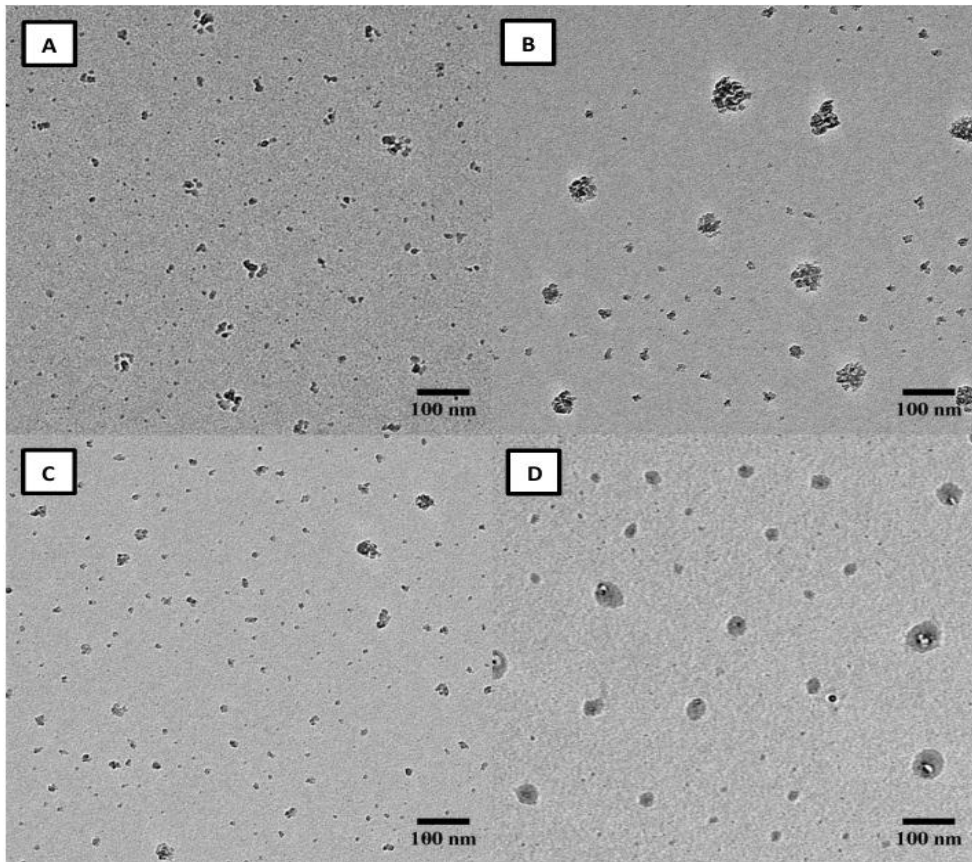


Figure 43: TEM Images of ash particles at 250 N-m, 1400 RPM

Table 8 shows the mass weighted distribution of elements based on EDS analysis of the TEM grids. A background subtraction method has been used to distinguish particles from grid background.

Table 8: EDS analysis - element weight percentage (Average of 30 samples)

Element	Weight (%) $\pm$ Std. Deviation (%)
Calcium	34.9 $\pm$ 17.0
Fluorine	8.3 $\pm$ 4.8
Oxygen	50.9 $\pm$ 20.5
Chlorine	2.0 $\pm$ 0.2
Phosphorus	3.9 $\pm$ 5.3



Lube oil analysis shows that the principle metal in commercial lube oils is calcium. Other work on engine ash composition shows that typically calcium sulfate and zinc phosphate are the main components of ash (Sappok et al., 2009). The John Deere oil used for the experiments has been sent for analysis. Table 9 shows a typical lube oil composition.

Table 9: Typical lube oil composition in PPM

<b>Elements</b>	<b>Castrol VW fresh lube oil (Gladis, 2010)</b>	<b>Fresh SAE 15W-40 (Sappok &amp; Wong, 2007)</b>
Ca	2996	2395
Mg	10	302
P	899	1244
S	4871	0.328%
Zn	963	1460
B	< 5	-
Fe	1	0
Si	3	4
Na	11	-

Chemical equilibrium calculations by Gladis (2010) show that calcium sulfate should be converted to calcium oxide (CaO) in the oven. Consequently it was expected that calcium oxide would be the main constituent of ash leaving the oven. The EDS analysis shows that calcium is a major constituent but there is a surprising amount of oxygen. The ratio of oxygen to calcium by mass in CaO is 0.40 but the ratio on the grid is 1.46 so there is much too much oxygen. Quantification of oxygen from EDS analysis is difficult for several reasons:

1. Oxygen is present on the TEM grid due to oxidation of carbon and the manufacturing process involved in making the TEM grid.
2. The oxygen percentage on TEM grids varies with the production batch and thickness of the grids.

3. Copper present on the grid contains a layer of copper oxide.
4. It was difficult to find a particle free spot on engine ash samples with the TEM for EDS analysis.
5. Silicon on the blanks in the form of silicon dioxide also contributes to the oxygen present

A further issue is difficulty with the background subtraction. An approximate method was used to correct the sample for background. The elements found in the blanks were carbon, silicon, oxygen and copper and are subtracted from the background for ash samples. Fluorine was also found in the sample. It might be attributed to fluorinated ZDDP present in the oil or contamination from fluorinated polymers found in the lab.

Figure 44 summarizes number, volume, mass weighted size distributions for engine exhaust at 250 N-m and 1400 RPM. The ash emissions were found to be  $44.3 \pm 1.5 \mu\text{g}/\text{m}^3$  and the ash fraction was found to be  $0.3\% \pm 0.1\%$ . This is close to 0.5%-1.5% ash fraction found in literature.

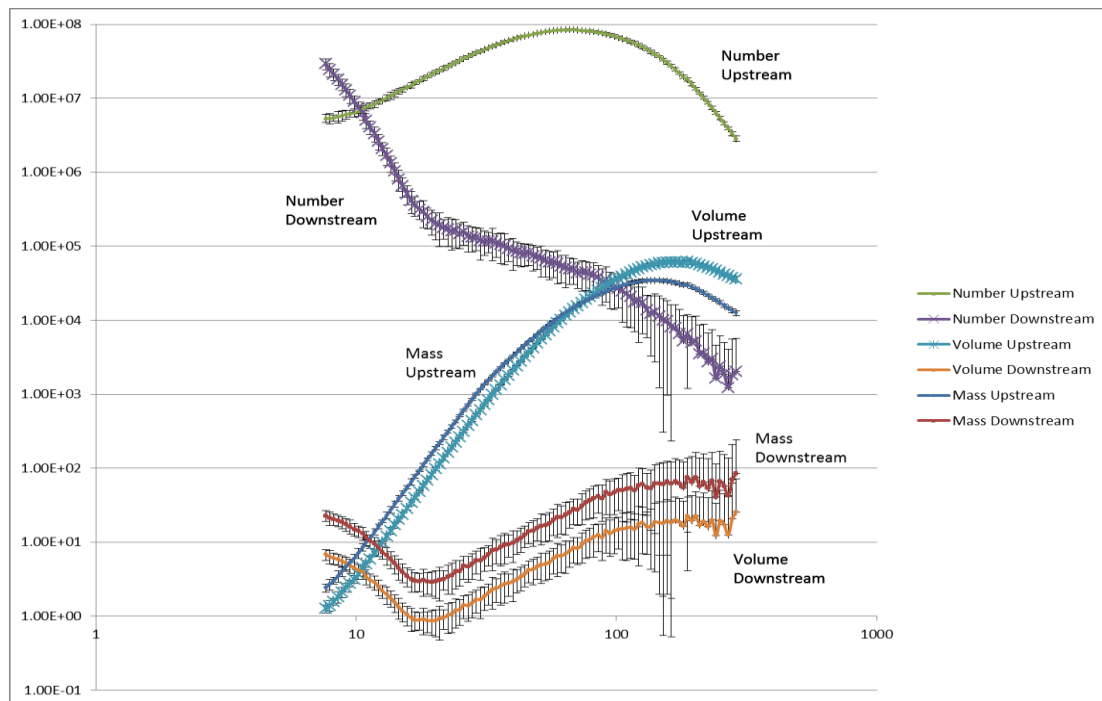


Figure 44: Number, volume and mass weighted size distributions for engine exhaust at 250 N-m and 1400 RPM

## Chapter 5: Conclusions and suggestions for future work

### 5.1 Conclusions

Each of the objectives of this work is listed below along with a summary of how it was achieved.

1. Develop a sampling system to collect unbiased particle samples for TEM analysis.

The objective of collecting an unbiased sample of the aerosol was accomplished by designing and building a thermal sampler based on work of Lorenzo et al. (2007). The new design provided a temperature gradient of  $3 \times 10^5$  K/m and better temperature control.

2. Understand the morphology of ash produced from the oil spray experiments.

Lube oil spray experiments were helpful in provided insights on the morphology of the ash particles generated from lube oil containing different additive packages. TEM images for the calcium additized oils 100A (Ca/P/S) and 102A (Ca/S) displayed similar particle morphology and a diameter range of 5-40 nm. EDS analysis of sample 100A (Ca/P/S) and 102A (Ca/S) showed the presence of calcium in the sample. The particles formed for 100A (Ca/P/S) and 102A (Ca/S) are likely calcium oxide particles. For the zinc additized oil 101A (Zn/S/P), the particles deposited on the grid are smaller, spherical, and in the range of 5-20 nm. The magnesium additized oil 103A (Mg/B) shows particle size in the range of 5-30 nm. EDS analysis of 101A (Zn/S/P) and 103A (Mg/B) did not yield any results as the mass concentrations on the grids were below the lower detectability limits of the EDS.

3. Perform calibration experiments to measure the survival of different ash constituents.

Calibration experiments for measuring survival fraction of different additives were conducted using aqueous salt spray experiments. For the aqueous salt spray experiments, salts of calcium, magnesium and zinc were atomized in water solutions and particle concentrations measured upstream and downstream of the oven. Volume survival fraction for the salts were found to be 54.7% for  $\text{CaSO}_4$ , 34.6% for  $\text{MgSO}_4$ , 26% for  $\text{Zn}_3(\text{PO}_4)_2$  and 7% for  $\text{ZnSO}_4$ .

4. Collect samples of engine exhaust particles upstream and downstream of the HTM oven and determine the morphology of the ash and its chemical composition.

The ash samples were collected at a load of 250 N-m and 1400 RPM. Figure 44 summarizes the number, volume and mass weighted size distribution for the engine exhaust. The TEM samples showed particles in the size range 5-100 nm and EDS analysis indicated that they consisted of mainly calcium and oxygen. EDS results could not be for quantification due to difficulty in background correction on the samples.

5. Use calibration results to correct engine ash concentrations measured downstream of the HTOM oven back to engine tailpipe conditions.

The SMPS measurements were used to measure upstream and downstream number and volume concentration. The downstream measurements were corrected for losses assuming CaO was the main ash constituent and indicated an exhaust ash content of  $44.3\mu\text{g}/\text{m}^3$  which corresponds to about 0.3 % of the exhaust PM.

## 5.2 Suggestions for future work

Although significant improvements were made in HTOM, there is still some scope for further improvements with the setup and the procedure. They are as follows:

- To identify whether carbon is penetrating the oven, it is important to do TEM and EDS analysis of the ash on TEM grids which do not contain carbon in the background. Grids composed of silicon dioxide would be suitable for this purpose.
- EDS could be used as a tool for quantitative analysis if enough samples are collected. A systematic method needs to be deployed to correct for the background on TEM samples with reasonable accuracy. However, EDS analysis is a time consuming process.
- Conduct TEM analysis at higher resolution to understand the morphology of ash and soot samples in greater detail.
- Aqueous spray experiments should be conducted with mixtures of salts in a elemental ratio similar to specially blended lube oils. The results can then be compared to lube oil spray experiment results and the differences in penetration can be studied.
- Additional engine studies should be performed at more steady state and transient engine conditions.

## **Bibliography:**

Andrews, G., Elamir, I., Abdelhalim, S., Ahamed, F. et al., The Measurement of Lubricating Oil Combustion Efficiency Using Diesel Particulate Analysis, SAE Technical Paper 980523, 1998. Liati, A., Dimopoulos Eggenschwiler, P., Müller Gubler, E., Schreiber, D., Aguirre, M., Investigation of diesel ash particulate matter: A scanning electron microscope and transmission electron microscope study, Atmospheric Environment, , 2012.

Apple, J., Gladis, D., Watts, W., and Kittelson, D., Measuring Diesel Ash Emissions and Estimating Lube Oil Consumption Using a High Temperature Oxidation Method, SAE Int. J. Fuels Lubr. , 2009.

Asseff, P.A., ZnDTP, U.S. Patent 2,261,047, Lubrizol 1941,.

Bardasz, E., Cowling, S., Panesar, A., Durham, J., Tadrous, T, Effects of Lubricant Derived Chemistries on Performance of the Catalyzed Diesel Particulate Filters, SAE Technical Paper , 2005.

Barris, M.A., Reinhart, S.B, and Wahlquist, F.H., The influence of Lubricating Oil and Diesel Fuel on Ash Accumulation in an Exhaust Particulate Trap, SAE Technical Paper , 1991.

Boonchom, B., Baitahe, R., Kongtaweelert, S., Vittayakorn, N., Kinetics and Thermodynamics of Zinc Phosphate Hydrate Synthesized by a Simple Route in Aqueous and Acetone Media, Ind. Eng. Chem. Res., 2010.

Bodek, K. and Wong, V., The Effects of Sulfated Ash, Phosphorus and Sulfur on Diesel Aftertreatment Systems - A Review, SAE Technical Paper , 2007.

Chamberlin, W. B. and Zalar, F. V., Balancing Crankcase Lubricant Performance with Catalyst Life, SAE Paper , 1984

Filice, M., W. Watts, and D. Kittelson., Near RealTime Ash Measurement. A Preliminary Study,, 2007.

Fritzsche, G. and Gerve, A., "Die Verfahren der Radionuklidtechnik für Ölverbrauchsmessungen," Motortechnische Zeitschrift, vol. 41 (1980)

Gardiner, E. and Denison, G. H., "Compounded Mineral Oil," U.S. Patent 2,211,972, , Chevron, 1940.

Givens, W.A., et al. "Lube formulation effects on transfer of elements to exhaust after-treatment system components," SAE International, 2003.

Gladis, D., Real time method of making engine ash emissions measurement, M.S Thesis, 2010.

Hinds, William C. Aerosol Technology : Properties, Behavior, and Measurement of Airborne Particles. 2nd ed. New York: Wiley, 1999.

Mu , J., and Perimutter, D.D, " Thermal Decomposition of Inorganic Sulfates and Their Hydrates", Ind. Eng. Chem. Process Des. Dev., 1981.

Jung H., David B. Kittelson, Michael R. Zachariah, "The influence of a cerium additive on ultrafine diesel particle emissions and kinetics of oxidation", Combustion and Flame, Volume 142, April 2005, Pages 276–288

Jung H., Kittelson, D., Zachariah, M., Kinetics and visualization of soot oxidation using transmission electron microscopy Combustion and Flame, 2004

Jung, H., Kittelson, D., and Zachariah, M., "The Influence of Engine Lubricating Oil on Diesel Nanoparticle Emissions and Kinetics of Oxidation," SAE Technical Paper, 2003

Ishiguro, T., Takatori, Y., Akihama, K., Microstructure of diesel soot particles probed by electron microscopy: First observation of inner core and outer shell, *Combustion and Flame*, 1997

Kim, J., High Temperature Oxidation Method for Real Time Measurement of Metallic Ash in Diesel Exhaust, MS University of Minnesota, 2005.

Kimura, K., Lynskey, M., Corrigan, E., Hickman, D. ., "Real World Study of Diesel Particulate Filter Ash Accumulation in Heavy-Duty Diesel Trucks," SAE Technical Paper , 2006

I.S. Abduhl-Khalek, Kittelson, D.B., Real Time Measurement of Volatile and Solid Exhaust Particles Using a Catalytic Stripper, SAE Paper, 1995.

Kittelson, D.B., Engines and nanoparticles: a review, *Journal of Aerosol Science*, 1998.

Konstandopoulos, A., Zarvalis, D., Kladopoulou, E., and Dolios, I.: A Multi-Reactor Assembly for Screening of Diesel Particulate Filters, 2006

Lee, K., Cole, R., Sekar, R., Choi, M. et al., Detailed Characterization of Morphology and Dimensions of Diesel Particulates via Thermophoretic Sampling," SAE Technical Paper, 2001

, Mang, V., Bobzin, T., Bartels, K.T., *Lubricants*, Wiley-VCH Verlag GmbH & Co. KGaA, *Industrial Tribology* , 2010.

Lorenzo, R. , Kaegi, R., Gehrig, R., Scherrer, L., Grobéty, B., Burtscher , H., A Thermophoretic Precipitator for the Representative Collection of Atmospheric Ultrafine Particles for Microscopic Analysis, *Aerosol Science and Technology* , , 2007



Manufacturers of Emission Controls Association (MECA), Diesel Particulate Filter Maintenance: Current Practices and Experience, Washington D.C., 2005.

Mayer, A. C., Ulrich, A., Czerwinski, J., and Mooney, J.J., Metal-Oxide Particles in Combustion Engine Exhaust, SAE Technical Paper , 2010.

McGeehan, J.A., Yeh, S., Couch, M., Hinz, A., et al., On the road to 2010 Emissions: Field Test Results and Analysis with DPF-SCR system and Ultra-Low-Sulfur diesel fuel, SAE Technical Paper, 2005

McGeehan, J., Van Dam, W., Narasaki, K., Boffa, A. et al., "Extending the Boundaries of Diesel Particulate Filter Maintenance With Ultra-Low Ash - Zero-Phosphorus Oil," SAE Int. J. Fuels Lubr 2012.

Nemoto, S., Kishi, Y., Matsuura, K., Miura, M. et al., Impact of Oil-derived Ash on continuous Regeneration- type Diesel Particulate Filter – JCAPII Oil WG Report, SAE Technical Paper, 2005.

Sappok, A., Santiago, M., Vianna, T., and Wong, V., Characteristics and Effects of Ash Accumulation on Diesel Particulate Filter Performance: Rapidly Aged and Field Aged Results, SAE Technical Paper , 2009.

Sappok, A., Wong, V., Detailed chemical and physical characterization of ash species in diesel exhaust entering after treatment systems, SAE International, World Congress, 2007.

Sappok, A., Rodriguez, R., and Wong, V., Characteristics and effects of lubricant additives chemistry on ash properties impacting diesel particulate filter service life, SAE International, 2010.

Thorsten Bartels et al., "Lubricants and Lubrication", Ullmann's Encyclopedia of Industrial Chemistry, 2005.

Takeuchi, Y., et al., The impact of diesel engine lubricants on deposit formation in diesel particulate filters, SAE International spring fuels and lubrication meeting, Yokohama, Japan, 2003

Vander Wal, R.L., and Mueller, C.J., Initial Investigation of Effects of Fuel Oxygenation on Nanostructure of Soot from a Direct-Injection Diesel Engine, Energy & Fuels, 2006 .

Young, D., Hickman, D., Bhatia, G., and Gunasekaran, N. "Ash Storage Concept for Diesel Particulate Filters," SAE Paper, 2004.

## Appendix I

Part drawings of the thermal sampler

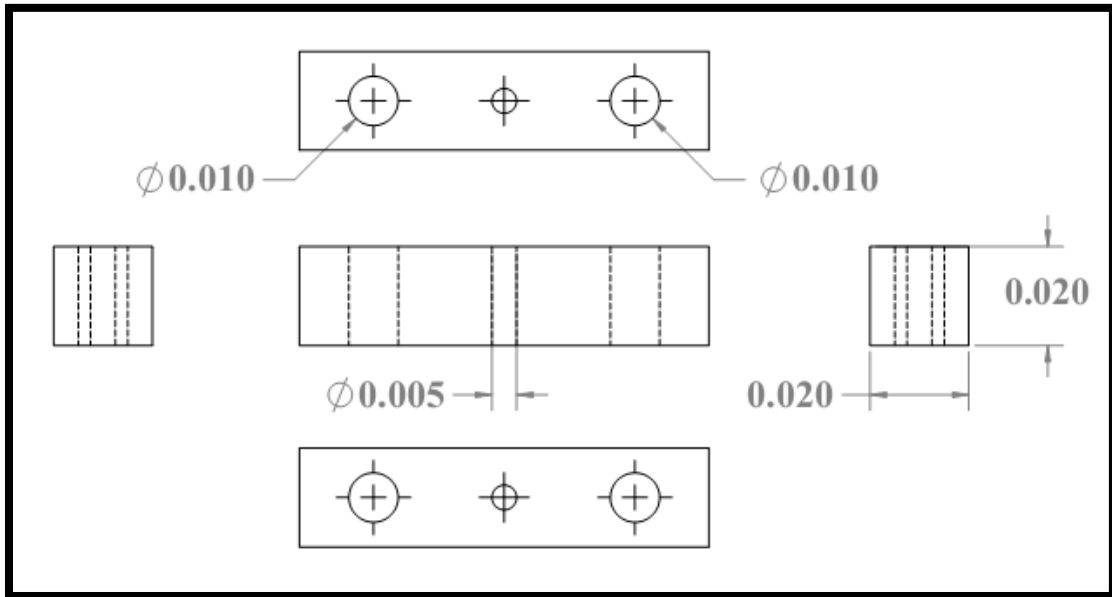


Figure 45: Top part of the thermal sampler

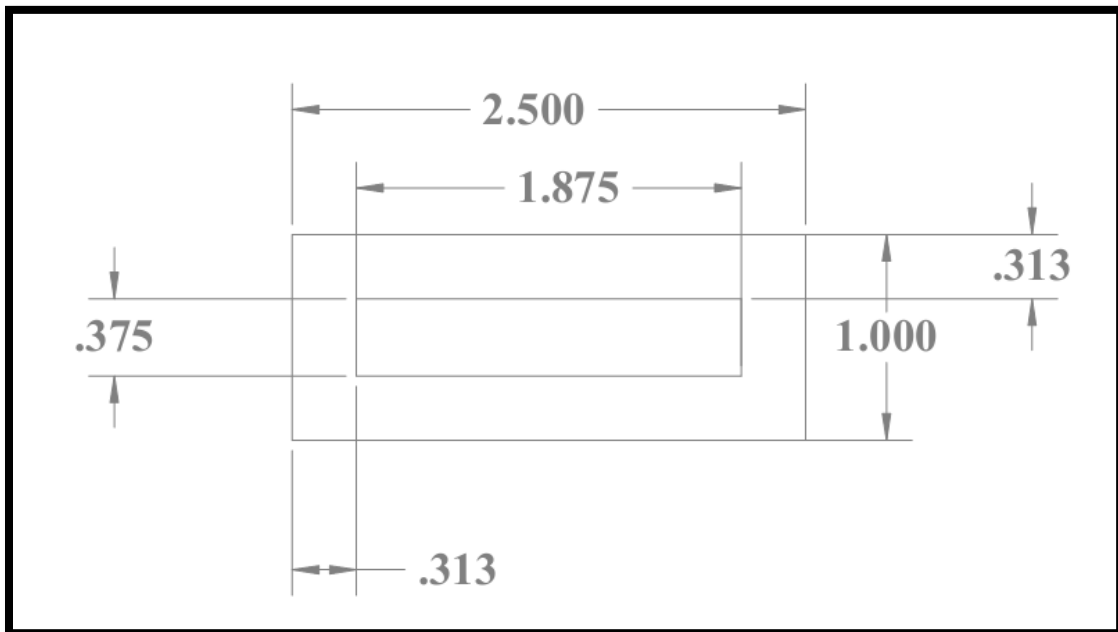


Figure 46: Brass plate used between the two blocks

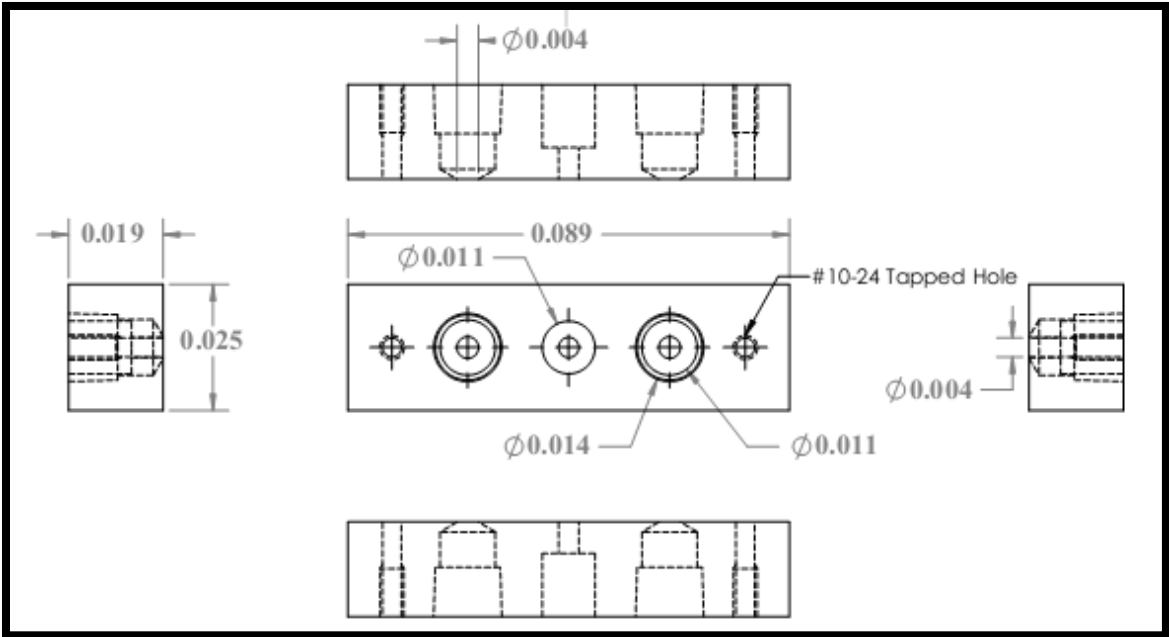


Figure 47: Bottom part of the thermal sampler

## Appendix II

Table 10: Test matrix

<b>Experiment</b>	<b>Oven Temperature</b>	<b>Repetitions</b>	<b>TEM Samples</b>
Lube oil spray [100A,101A,102A,103A]	1150°C	3 for each oil	2 for each oil
Aqueous salt spray [CaSO <sub>4</sub> , MgSO <sub>4</sub> , ZnSO <sub>4</sub> , Zn <sub>3</sub> (PO <sub>4</sub> ) <sub>2</sub> ]	800°C	3 for each salt	N/A
	1150°C	3 for each salt	N/A
Engine ash	1150°C	3	3

### Appendix III

Correction factor for thermophoretic losses

Thermophoretic losses occur when there is a temperature gradient. It can be corrected using equation 3,

$$\left( \frac{n_o}{n_i} \right) = \left( \frac{T_o}{T_i} \right)^{\text{Pr} K_f}$$

Equation 3: Thermophoretic Loss Correction

Where  $n_o$  is the concentration at temperature  $T_o$  and  $n_i$  is the concentration at temperature  $T_i$ .

## Appendix IV

Zinc phosphate aqueous spray: TEM and EDS analysis results

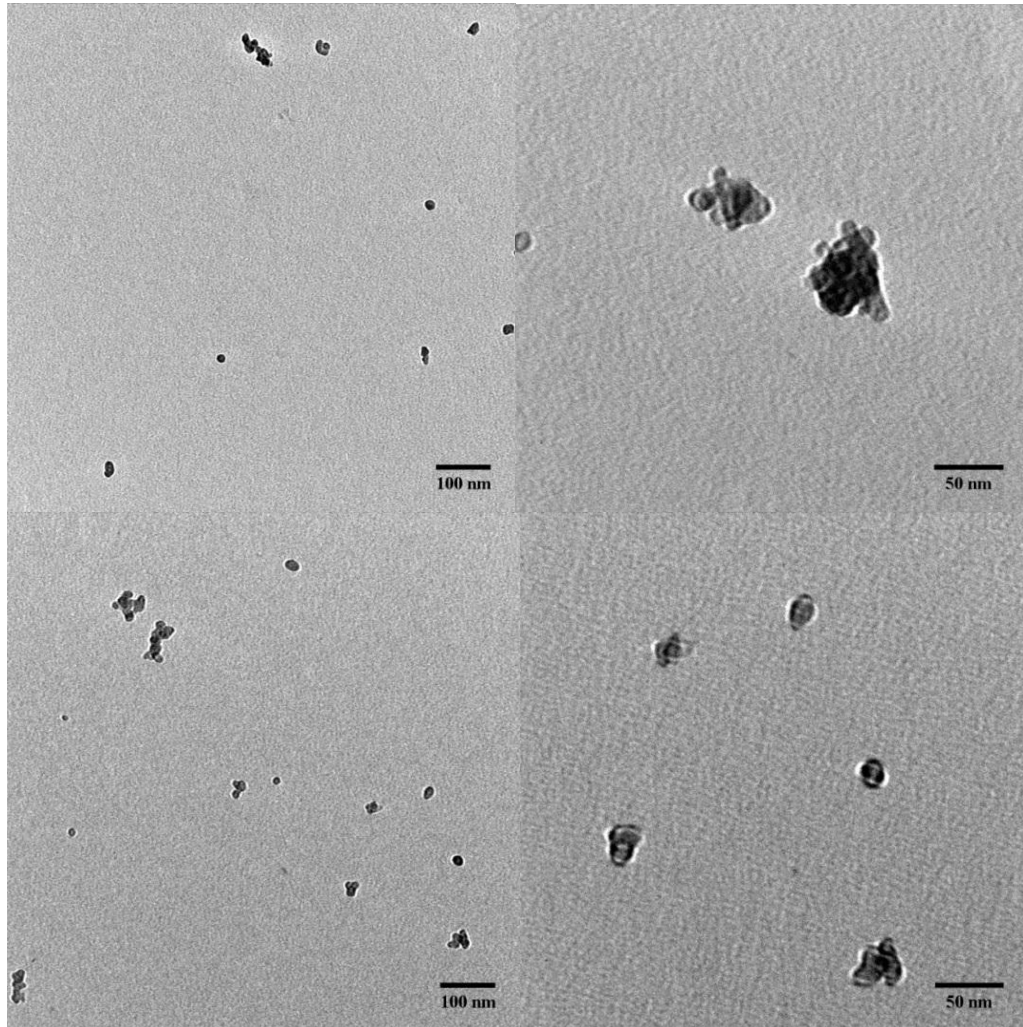


Figure 48: TEM images of zinc phosphate spray

Table 11: Results of EDS analysis for zinc phosphate sprays

O	Na	Si	P	Cl	K	Ca	Zn
68.68	3.32	1.45	6.65		0.6	1.11	18.19
79.28		1.84	5.58	0.66		0.74	11.9